



HAL
open science

Influence of SIC control rod material on the iodine release in case of nuclear severe accident – Chemical reactivity with fission products in thermal conditions of RCS

Anne Cecile Gregoire, Sophie Sobanska, Calogero Tornabene, David Talaga,
Anne-Sophie Mamede, Sandrine Morin, Laurent Cantrel

► To cite this version:

Anne Cecile Gregoire, Sophie Sobanska, Calogero Tornabene, David Talaga, Anne-Sophie Mamede, et al.. Influence of SIC control rod material on the iodine release in case of nuclear severe accident – Chemical reactivity with fission products in thermal conditions of RCS. *Annals of Nuclear Energy*, 2021, 168, pp.108900. 10.1016/j.anucene.2021.108900 . hal-03536395

HAL Id: hal-03536395

<https://hal.science/hal-03536395>

Submitted on 19 Jan 2022

HAL is a multi-disciplinary open access archive for the deposit and dissemination of scientific research documents, whether they are published or not. The documents may come from teaching and research institutions in France or abroad, or from public or private research centers.

L'archive ouverte pluridisciplinaire **HAL**, est destinée au dépôt et à la diffusion de documents scientifiques de niveau recherche, publiés ou non, émanant des établissements d'enseignement et de recherche français ou étrangers, des laboratoires publics ou privés.

1 **Influence of SIC control rod material on the iodine release in case of nuclear**
2 **severe accident – Chemical reactivity with fission products in thermal**
3 **conditions of RCS**

4 A.C. Grégoire^a, S. Sobanska^b, C. Tornabene^a, D. Talaga^b, A.S. Mamede^c, S. Morin^a, L. Cantrel^a.

5 ^a Institut de Radioprotection et de Sûreté Nucléaire, Pôle Sûreté Nucléaire, CEN Cadarache, Saint Paul
6 lez Durance F-13115, France

7 ^b Institut des Sciences Moléculaires, Université de Bordeaux, UMR5255 CNRS, 33405 Talence cedex
8 France

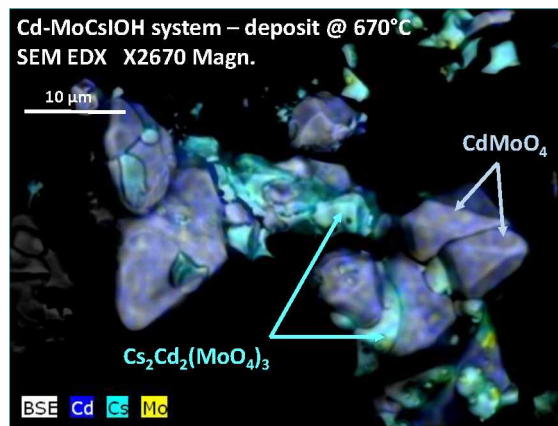
9 ^c Unité de Catalyse et Chimie du Solide, Université de Lille, CNRS, Centrale Lille, Université d'Artois,
10 UMR 8181, F-59000 Lille, France

11

12

13

14 **Graphical abstract**



15

16

17 **Abstract**

18 The effect of Silver-Indium-Cadmium (SIC) control rod on the transport of volatile fission products (I,
19 Cs, Mo) in conditions of a Reactor Coolant System under NPP severe accident was investigated within
20 three semi-integral tests in a thermal gradient tube. The experiments addressed separately the effect
21 of each SIC element. Nature of transported and deposited species was investigated by ICP MS, ESEM-
22 EDX, Raman Microspectrometry, XRD and XPS techniques.

23 For the first time, numerous metallic molybdates involving SIC components were evidenced. The
24 formation of such metallic molybdates competes with the formation of Cs-molybdate and may in
25 certain conditions strongly reduce the scavenging effect of Mo towards Cs. As a result the nature of
26 transported iodine can be strongly modified, compared to chemical systems involving only Mo, Cs and
27 I. The data obtained are useful to guide what species have to be added in the thermodynamic database
28 used in the SA simulation software.

29

30 **Keywords:**

31 Severe accident, Reactor Coolant System, Metallic molybdates, Chemical reactivity, Iodine transport

32

33 **Highlights:**

34 The SIC components reacts with Mo oxide to form metallic molybdates

35 With respect to Mo oxide, SIC components can be ordered by increasing reactivity: In < Ag ~ Cd

36 The formation of SIC metallic molybdates competes with Cs-scavenging effect of Mo oxide

37 The presence of SIC elements has a strong influence on the nature of iodine released from the RCS

38

39 1. Introduction

40 During a severe accident (SA) occurring on a nuclear power plant (NPP), strong releases of volatile
41 fission products (FPs) such as iodine, caesium or even molybdenum are expected. These FPs can
42 contribute to high radiological consequences in case of releases into the environment following early
43 containment venting procedure or containment failure - as was the case during the Fukushima Daichi
44 NPP accident (Masson *et al.*, 2011; Chino *et al.*, 2011; Huh *et al.*, 2012; Stohl *et al.*, 2012; Lebel *et al.*,
45 2016). In such situation, the accident management is strongly linked to the physico-chemical forms of
46 the released radioisotopes, especially for iodine as gaseous or particulates species do not contribute
47 to the same extent to radiological consequences (Hoeve and Jacobson, 2012; Geng *et al.*, 2017; Masson
48 *et al.*, 2019).

49 In early accidental phase, the nature of the radioisotope released from the Reactor Coolant System
50 (RCS) and accumulated in the nuclear containment building is directly linked to the physico-chemical
51 phenomena prevailing in the RCS. Little information is available in the literature concerning the
52 chemical speciation inside the RCS (Clément *et al.*, 2007). The phenomena occurring in the RCS during
53 a SA are indeed very complex involving strong thermal gradients, rapid atmosphere changes from
54 reducing to oxidizing conditions, complex chemical systems involving some more or less volatile FPs
55 (Cs, I, Mo, Te), control rod (CR material such as Ag, In, Cd and B) and structure materials with release
56 kinetics and thus element ratio depending on the extent of fuel degradation.

57 The chemical form of iodine and its behaviour after entering containment from the RCS break were
58 previously documented in NUREG/CR-5732 (Beahm *et al.*, 1992). On the basis of thermodynamic
59 computation it was considered that iodine entering the containment was at least 95 % under CsI form
60 with the remaining 5% as I and HI under gaseous form. For caesium, the main prevailing assumption is
61 that the CsOH is in large excess (Williams, 1994). After extensive experimental research and modelling
62 on fission product release and transport in severe accident conditions over the past thirty years, the
63 situation appears much more complex.

64 Indeed the large scale Phébus FP test series showed that in addition to CsI, other condensable iodide
65 forms may exist in the RCS (Girault and Payot, 2013). Indeed, the deposits collected on the thermal
66 gradient tubes (700 -150°C temperature range) of the Phébus experimental circuit and determined by
67 γ -spectrometric measurements presented several iodine condensation peaks not systematically
68 correlated to caesium deposit. Moreover, the fractions of aerosol/gaseous iodine transported into the
69 Phébus containment vessel (150°C) were variable and strongly dependent on the test scenario (Girault
70 *et al.*, 2010, Girault *et al.*, 2012, Haste *et al.*, 2013), suggesting a complex chemistry during the transit
71 though the experimental circuits. In addition, the small-scale Falcon ISP1/2 tests performed with
72 simulatant fuel pellets (Williams, 1994) and VERCORS HT2/3 tests performed with actual spent fuel
73 pellets (Pontillon and Ducros 2010) supported also the assumption of iodine being transported in
74 others forms than CsI; CdI_2 is suggested as a possible alternative. Deposition profile of the other main
75 released FPs (Mo, Cs, Te ...) and CR elements (Ag, In, Cd) in the thermal gradient was also determined
76 for these tests either by γ -spectrometry (VERCORS HT test) or after chemical leaching and elemental
77 analysis (ICP OES – Falcon tests) . Based on the elements condensation peaks, the formation of various
78 metallic molybdates were put forward (McFarlane *et al.*, 2002) as well as the formation of CsTe species
79 (McFarlane and Leblanc, 1996; De Boer and Cordfunke, 1995) supporting the fact that caesium
80 chemistry is also more complex than initially expected. The formation of caesium borates was also
81 assumed based on separate effect tests (Bowsher and Nichols, 1985; Bowsher and Diskinson, 1986;
82 Elrick *et al.*, 1987) but boron deposition profile could not be determined (no γ -emitter). The use of
83 actual spent fuel for such experiments allows to be as close as possible of a reactor case but induces
84 experimental issues due to the handling of highly reactive samples. As a consequence, the
85 characterization of the deposited/transported material was limited mainly to γ -spectrometry which
86 cannot provide any chemical speciation. Interpretation of such experiments relies thus mostly on
87 computer simulations which in turn needs reliable thermodynamic and thermokinetic data for

88 chemistry of FPs and CR material at high temperature, even if recent works were performed to improve
89 these data (Grégoire *et al.*, 2017; Miyahara *et al.*, 2019) works are still ongoing on this.

90 In order to improve the understanding of the main chemical formation, decomposition, deposition
91 processes in which released FPs and control rod elements are involved in the RCS during a SA and also
92 to build an experimental database allowing the validation process for models, the ISTP-CHIP (2005-
93 2012) and the follow-up CHIP+ (2012-2018) experimental programs were launched at IRSN (Clement
94 and Zeyen, 2005). The CHIP (Chemistry Iodine Primary circuit) experimental set-up and its small scale
95 GAEC (Generation of AErosols in the reactor Coolant system) analog were designed as open flow
96 reactors in which reagents are continuously mixed at high temperature (1600°C) and transported into
97 a controlled thermal profile using carrier gas (steam/H₂) reproducing as much as possible conditions
98 of the RCS of a Light Water Reactor (LWR) during a SA. Chemical systems involving iodine, main
99 released FPs which can interfere with iodine (Cs and Mo) and control rod material (B, Cd, Ag and In)
100 were considered. Tellurium was not retained as this FP is about 5 times less abundant than Cs in the
101 spent fuel (Jacquemain *et al.*, 2000; Grégoire *et al.*, 2008) and is not expected to have a significant
102 influence on Cs reactivity. Only the natural stable isotopes of these elements were handled for safety
103 consideration. One of the main issues was to achieve element concentrations and relative ratio as
104 relevant as possible of conditions of interest. Deposited species, transported aerosols and gases were
105 collected for off-line characterization with a focus on gaseous iodine quantification. Working with
106 stable elements allowed involving various surface analytical techniques capable to unravel the nature
107 of deposited and transported species that could not be applied for experiments with highly radioactive
108 material. The studied chemical systems involved firstly only iodine with carrier gas (the I-O-H system)
109 and were then extended to other main FPs (Cs, Mo) and Cr materials involving up to 7 elements
110 (Grégoire *et al.*, 2018).

111 The experiments performed on the I-O-H system evidenced kinetic limitations for gas phase iodine
112 reactivity (Grégoire *et al.*, 2017). The addition of caesium, in quite large excess relative to iodine to be
113 relevant of severe accident scenarios, resulted in quantitative formation of caesium iodide, preventing
114 thus any gaseous iodine transport whatever the gas atmosphere (steam or steam/hydrogen). No
115 relevant kinetic limitations were evidenced (Grégoire *et al.*, 2015), so the main caesium species (CsI,
116 CsOH) can be simulated with the thermodynamic equilibrium assumption. Mo is expected to act as a
117 Cs sink by the formation in the gas phase of stable caesium molybdates as expected by
118 thermochemical data (Tangri *et al.* 1989; Cordfunke and Konings, 1990) which then condenses on the
119 colder parts of the RCS. The formation of caesium molybdates of various composition could be clearly
120 identified in the deposits collected in the test lines (Lacoue-Nègre, 2010; Gouello *et al.*, 2013; Grégoire
121 *et al.*, 2015) when both Mo and Cs were considered. The reactivity of the Mo-Cs-I-O-H system is quite
122 well reproduced by simulation tools and its consequence on iodine transport well predicted both in
123 reductive or oxidative atmosphere. First results obtained from the B-Cs-I-O-H systems tends to show
124 that the formation of caesium borates is less favourable (Gouello, 2012; Grégoire and Mutelle, 2012).

125 As a follow up to the test performed only with the main FPs, the study of the extended systems
126 addressed separately the influence of each element of the Silver-Indium-Cadmium control rod
127 compared to tests performed with the Mo-Cs-I-O-H system in steam condition. In steam condition, we
128 have demonstrated that the formation of stable caesium molybdates prevents CsI recombination and
129 thus enhance the release of gaseous iodine (Grégoire *et al.*, 2015). On the contrary, silver, indium and
130 cadmium (SIC) are expected to react with iodine to form metallic iodide (AgI, CdI₂ and possibly InI_x
131 species). Nevertheless, the formation of metal-molybdates is not excluded that would compete either
132 with metal iodide or caesium molybdate generation.

133 Within that context this work aims at evaluating the chemical reactivity between FPs (I, Cs and Mo)
134 and SIC control rod material (either Ag, or In or Cd) in thermal conditions of a RCS in order to highlight
135 the role of SIC in the release of gaseous iodine during a SA. The main objective was to assess the
136 influence of each additional element (Ag, In, Cd) on the nature of deposited and transported species
137 compared to the Mo-Cs-I-O-H chemical system alone. A special attention was brought on the

138 formation of metallic iodide and metallic molybdates which may play a key role on gaseous iodine
 139 persistence at 150 °C. Three tests were performed; each based on the Mo-Cs-I-O-H system in steam
 140 conditions plus one element of the SIC control rod: the [In+MoCsI] test, the [Cd+MoCsI] test and finally
 141 the [Ag+MoCsI] test. We are thus presenting the main results obtained from the extended system test
 142 series with a special attention on the determination of the deposited and transported species.

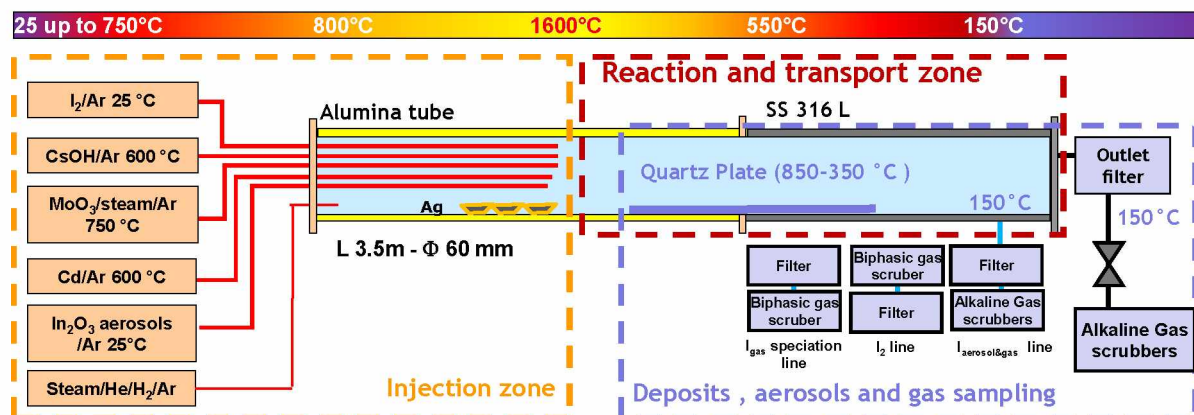
143 Hereafter, the CHIP experimental set-up, the test conditions and post-test operations including the
 144 analytical techniques dedicated to species identification will be detailed. Experimental results will be
 145 focused on element transport in the CHIP line with a special attention on iodine behaviour and the
 146 identification of the condensed species. Discussion will be held in comparison with literature data.

147 2. Material and methods

148 2.1 CHIP Line description

149 The CHIP line has been described previously (Grégoire *et al.*, 2012; 2015; 2018) so that only features
 150 concerning injection of I, Cs, Mo plus Cd, In and Ag will be detailed here.

151 The test line (3.5 m long and 60 mm in internal diameter) is composed of two tubes assembled by
 152 a specific junction (Figure 1): an alumina tube (2 m) located in the high temperature zone and a
 153 stainless steel tube (1.5 m) in the transport zone - simulating RCS piping. The thermal profile is obtained
 154 by mean of several furnaces (High temperature tri zone CARBOLITE furnace completed by a series of
 155 WATTLOW ceramic heaters) and is composed of three zones (injection zone, reaction zone and
 156 aerosol/deposit and gas collection zone). Thermal profile is obtained after ~20-24 h of slow heating.
 157 Residence time (10-11 s) from the high temperature zone to the outlet is representative of an accident
 158 scenario featuring a break in the cold leg of the RCS.



159
 160 *Figure 1: CHIP line configuration for injection of Ag, In and Cd*

161 In order to allow working with various chemical systems featuring a wide range of concentrations and
 162 elemental ratio, elements are injected either in their metal, oxide or hydroxide form, depending on
 163 their stability and volatility. One major issue to be addressed was the achievement of a controlled
 164 injection of cadmium (as Cd metal), indium (as In₂O₃ powder) and silver (as Ag metal) so as to achieve
 165 concentrations and ratios relative to iodine relevant of an accidental scenario as observed during the
 166 Phébus FP tests (Grégoire et Haste, 2013, Haste *et al.*, 2013, Girault and Payot, 2013). Several years of
 167 development were necessary to succeed injecting those refractive and poorly soluble elements in a
 168 controlled way.

169 Except for silver, vapours or aerosols are produced by the mean of external generators connected
 170 to the inlet flange. The carrier gas (steam/Ar or He) is directly injected at the main line inlet (800°C)
 171 whereas other reagents are transported directly into the high temperature zone via separate alumina
 172 nozzles. At 1600°C, all the injected species are under vapour form at thermodynamic equilibrium.
 173 Gaseous iodine is obtained by sublimation of molecular iodine pellets. Caesium, molybdenum and
 174 cadmium vapours are produced by vaporization of respectively caesium hydroxide, molybdenum

175 trioxide and metallic cadmium. Indium oxide vapours are obtained by the injection of dry indium oxide
176 aerosols produced at room temperature (RBG 1000 aerosol generator, PALAS) and then gradually
177 vaporised in the pre-heating zone. Being more refractive than the other elements, silver is directly
178 vaporised in the main line (at temperatures above 1200°C) from silver powder deposited in crucibles.
179 At steady state, these generators produce a stable mass flow rate of each reagent for several hours –
180 allowing thus the different sampling operations.

181 Apart from the carrier gas, at the outlet of the transport zone and in the sampling lines (150°C), only
182 iodine can be possibly found in gaseous form, the other elements (FPs simulant and CR material) being
183 transported as particulate material at this temperature level. In order to quantify the fraction of
184 gaseous iodine released at the outlet, the CHIP line is terminated by an integral aerosol filter followed
185 by gas scrubbers filled with an alkaline solution dedicated to trap gaseous iodine species and
186 condensed steam. The integral aerosol filter is composed of quartz fibre cartridge with 0.9 µm porosity
187 resulting in aerosol retention superior to 99.9%, for aerosol diameter ranging between 0.3 and 0.7 µm
188 (see Table S1 in SD). The line outlet collects transported species over the entire test. Several sampling
189 lines which can be sequentially operated, are also implemented on the CHIP experimental set-up.
190 These lines are connected to the main CHIP line just before the outlet filter (Figure 1) and dedicated
191 to sample a fraction (2 up to 8%) of the main flow at 150°C (temperature corresponding to a cold leg
192 break of a RCS). These lines can be operated for short period and are able to catch changes in the
193 transported flow depending on the test conditions. Different design have been developed to address
194 different sampling objectives:

- 195 • collection of the transported aerosols and quantification of the total released gaseous iodine
196 fraction. Such line is implemented with an inlet quartz fibre membrane filter (0.7 µm porosity
197 resulting in aerosol retention >99%, see Table S1) allowing to trap the transported aerosols and
198 downstream gas scrubbers filled with alkaline media (NaOH 0.1 M) in which all expected gaseous
199 iodine species are readily soluble allowing the quantification of the total iodine gaseous fraction.
200 Such line is labelled “I_{aerosol&gas} line”;
- 201 • determination of the gaseous iodine speciation (Gouello *et al.*, 2013, Grégoire *et al.*, 2015). The line
202 is still composed of an inlet filter but in this case, the gas scrubbers located downstream are filled
203 with a biphasic mix of toluene dedicated for I₂ trapping and diluted nitric acid (0.015 M) dedicated
204 for the other inorganic gaseous iodine species (e.g. HI, HOI) allowing to determine the composition
205 of the gaseous iodine fraction (molecular iodine vs other inorganic forms). Such line configuration
206 is labelled “I_{gas} speciation line”;
- 207 • quantification of molecular iodine in presence of reactive species. As mentioned by Gouello *et*
208 *al.* (2013), the drawback of the “I_{aerosol&gas} line” and “I_{gas} speciation line” is the possible loss of gaseous
209 iodine due to interactions between gaseous iodine and reactive aerosols trapped on the filter (e.g.
210 CsOH for instance). In order to address this difficulty, a third line configuration was developed in
211 which the flow composed of gaseous species and aerosols is directed in gas scrubbers filled with a
212 mix of toluene/diluted nitric acid. Molecular iodine is collected in the organic phase whereas
213 inorganic iodine species and other aerosols are trapped in the aqueous phase. The line is
214 terminated by a filter to trap the aerosols reminder. In such configuration, only the fraction of
215 molecular iodine can be determined. Such line design is labelled “I₂ line”.

216 The redundancy of information which can be gained from the different sampling lines allows to
217 characterize the iodine release at 150°C (gas/aerosol distribution, nature of gaseous iodine forms) with
218 a good reliability.

219 In addition to the sampling of material transported at 150°C, a quartz plate is inserted in the main line
220 for collecting condensed material in 850-350°C temperature range. Thus, two types of samples were
221 collected: (i) condensed phases deposited on quartz substrate (1 x 5 cm) between 850 and 350°C and
222 (ii) particles sampled at 150°C using a glass fibre filter.

223 Specification on line structure and chemical reagents are displayed in the supplementary information
224 data files (Table S1 and Table S2) as well as the thermal profile in the transport zone (Figure S1).

225 **2.2 Test conditions**

226 Three tests were performed consisting in injecting the Mo-Cs-I-O-H chemical system in steam as
227 previously described in Grégoire *et al.* (2015) (the [PL_MoCsI_3] test) plus one element representative
228 of the SIC control rod: the [In+MoCsI] test, the [Cd+MoCsI] test and finally the [Ag+MoCsI] test.

229 The [PL_MoCsI_3] test will serve as reference test; it featured steam atmosphere with a chemical
230 system involving an excess of Cs relative to I (Cs/I molar ratio of ~4) and Mo itself in excess relative to
231 Cs (Mo/Cs ~3) in the range of ratios observed during Phébus FP test sequences (Haste *et al.*, 2013). The
232 steam atmosphere is relevant of the Phébus test main release phase during which the transport of Cs,
233 I, Mo in the experimental circuit was observed (Grégoire and Haste, 2013). The thermal hydraulic
234 conditions simulate as close as possible a large RCS cold leg with high thermal gradient and short
235 residence time in the transport zone (Jacquemain *et al.*, 2015). Inert gas (Ar or He) was added to adjust
236 the residence time of elements in the CHIP line. In such conditions, formation of caesium molybdates
237 partially prevents CsI to be formed in the gas phase and contributes to the transport of high gaseous
238 iodine fraction (up to 90% of injected iodine mass, Grégoire *et al.*, 2015).

239 [In+MoCsI], [Cd+MoCsI] and [Ag+MoCsI] tests with extended chemical systems were performed with
240 similar element injection for Mo, Cs and I. The SIC CR elements were injected in large excess relative
241 to iodine. A similar thermal gradient and residence time was applied. As for the carrier gas
242 composition, a mix of steam/inert gas was injected for the [In+MoCsI] and [Cd+MoCsI] tests as it was
243 observed that those CR elements were also released during the Phébus tests main release phase (in
244 steam atmosphere). A low amount of hydrogen (1.8% of the total atmosphere) was added for the test
245 featuring silver, as this element was released later during the so-called “second oxidation phase”
246 where low amounts of H₂ were measured in the Phébus circuit (Grégoire and Haste, 2013).

247

248 The thermal hydraulic conditions and element generation are reported in Table 1. Conditions of the
249 reference [PL_MoCsI_3] test are recalled too. The element mean mass flow rates were determined
250 from the total injected element masses (based on the final element mass distribution in the line) and
251 the injection duration assuming a steady injection rate. Given uncertainty on ICP-MS analyses of each
252 leaching solution, an average uncertainty of +/-7 % could be estimated for the element mean mass
253 flow rate. As silver crucibles were placed directly in the main line, significant vaporization occurred as
254 soon as the temperature in the crucible reached ~ 1100 °C. As a consequence, injection of low silver
255 level in the line could not be avoided during the pre-heating phase, before injection of the other
256 elements. Given the relative short duration of this pre-heating phase and low carrier gas flow applied
257 during this phase, it is assumed that the main part of silver was injected during the main phase of the
258 test as the other elements. The silver mass flow rate (displayed in Table 1) was determined from the
259 overall silver mass collected in the CHIP line, including the deposits formed during the pre-heating
260 phase and should be thus considered as a maximal value.

261 *Table 1: Conditions of [In+MoCsl], [Cd+MoCsl] and [Ag+MoCsl] tests and [PL_MoCsl_3] reference test*

Test Name	[In+MoCsl]	[Cd+MoCsl]	[Ag+MoCsl]	[PL_MoCsl_3] (Grégoire et al., 2015).
Test Loop	CHIP PL			
Main test tube material	Alumina (HT zone – 600°C) / stainless steel (600°C-150°C)			
<i>Thermal hydraulic conditions :</i>				
Pressure (Mpa)	0.2 MPa			
Carrier gas flow (l/min – NPT)	38.2 l/min	35.3 l/min	35.1 l/min	34.3 l/min
Max. temperature in the HT zone (°C)	1600°C			
Temperature profile in the transport zone	Strong ∇ to outlet (150°C)			
Residence time in the transport zone (s)	~12 s			
Test duration (min)	357	337	338	421
<i>Carrier gas composition (v/v %)</i>				
	H ₂ O/Ar	H ₂ O/He/Ar	H ₂ O/Ar/H ₂	H ₂ O/He/Ar
	45.7/54.3	49.4/42.8/7.8	49.6/48.6/1.8	50.8/44.1/5.1
<i>Element injection</i> mean mass flow rate (mol/s) in the HT zone [†]				
Iodine (as I ₂)	1.8 10 ⁻⁷ mol/s	1.7 10 ⁻⁷ mol/s	1.5 10 ⁻⁷ mol/s	1.5 10 ⁻⁷ mol/s
Caesium (as CsOH)	4.4 10 ⁻⁷ mol/s	5.5 10 ⁻⁷ mol/s	5.6 10 ⁻⁷ mol/s	6.0 10 ⁻⁷ mol/s
Molybdenum (as MoO ₃)	2.2 10 ⁻⁶ mol/s	2.0 10 ⁻⁶ mol/s	2.1 10 ⁻⁶ mol/s	1.9 10 ⁻⁶ mol/s
Indium (as In ₂ O ₃)	8.1 10 ⁻⁷ mol/s	-	-	-
Cadmium (as Cd metal)	-	2.1 10 ⁻⁵ mol/s	-	-
Silver (as Ag metal)	-	-	7.4 10 ⁻⁶ mol/s ^a	-

262 NPT conditions: 0°C, 0.101325 MPa ; [†] Element flow rate based on the final mass distribution in the line and assuming a steady injection
 263 rate (relative uncertainties below $\pm 5\%$ except for iodine in the [Ag+MoCsl] test : $\pm 50\%$); ^a maximum flow rate as silver vaporization may
 264 also occur during the pre-heating phase.

265

266 **2.3 Element mass concentration and distribution along the thermal profile of CHIP line**

267 In order to determine the element distribution in the CHIP line, several successive washing operations
 268 were performed post-test to solubilize the deposited material. For the test series with injection of SIC
 269 control rod material, the following solutions were used:

- 270 • alkaline media (NaOH 0.1 M) for easily soluble species such as I₂, HI, HOI, Csl or Cdl₂ and partly
 271 caesium molybdates;
- 272 • nitric acid (2 M) for an overall recovery of molybdates (MoO₃, molybdic acid, metallic molybdates)
 273 and cadmium species (Cd metal, oxide and possibly hydroxide);
- 274 • nitric acid (5 M) for metallic silver;
- 275 • boiling concentrated nitric acid (8 M) for indium oxides.

276 A last treatment was necessary for AgI recovery as this species is still insoluble in concentrated acidic
 277 media. This treatment (Spies, 1936; Wang *et al.*, 1989) is based on the decomposition of AgI by hot
 278 aqua regia (1/3 nitric acid; 2/3 hydrochloric acid). In presence of a large excess of chlorides, the
 279 insoluble form of AgCl is favoured and I solubilized as iodine monochloride (ICl). The solution is then
 280 filtered and the filtrate treated with sodium hydroxide (final pH above 13) allowing to hydrolyse the
 281 iodine monochloride and form iodates and iodides. Analyses of solubilised iodine allows then to
 282 quantify the amount of silver iodide. No similar approach could be developed for Cdl₂/Csl separation
 283 and quantification due to their strong solubility in aqueous media. Formation of such species will be
 284 then deduced by default of other species.

285 The solutions were then analysed by multi-elemental analysis techniques: Inductively Coupled Plasma
 286 Mass-Spectrometry (ICP-MS) for I, Cs, Mo, Cd and In (Varian 810 MS) or Inductively Coupled Plasma
 287 Atomic Emission Spectroscopy (ICP-AES) for Ag (Perkin Elmer, 8100) with a relative uncertainty of +/-
 288 8% at 95% confidence level. UV-visible quantification of I₂ in toluene was performed with an Agilent
 289 8453 spectrometer at 309 nm and 498 nm with an uncertainty of +/- 6% (at 95 % confidence level).

290 **2.4 Characterization of collected material**

291 Material deposited in the thermal gradient onto quartz plate samples and aerosols collected on quartz
292 filters, were post-test analysed. Size and morphology have been determined by Environmental
293 Scanning Electron Microscopy (ESEM Quanta 200 FEI®) used in low vacuum mode (50-130 Pa), allowing
294 to examine sample without metallisation. Measurements were carried out at an accelerating voltage
295 of 10-25 kV to perform either Secondary electron or Back Scattering Electron (BSE) imaging with a
296 lateral resolution of several hundred of nm. Semi-quantitative elemental composition was obtained by
297 an energy-dispersive X-ray detector (EDX, Quantax-Roentec®) coupled to the ESEM microscope. ZAF
298 (Atomic Number Z, Absorption and Fluorescence) corrections were applied. Elemental composition of
299 single particles and cartography of larger zones (~20*20 up to 100*100 µm²) could be determined with
300 a resolution of ~1µm³. Raman microspectrometry (RMS) was performed on the same sample zones to
301 identify both elemental and molecular composition of condensed species. The Raman spectra and
302 optical images were recorded by Labspec6 using a confocal Raman microspectrometer (Labram HR
303 evolution, Horiba Jobin Yvon) equipped with a 100× 0.85 numerical aperture objective (Olympus). An
304 excitation Nd:YAG laser with a wavelength of 532 nm and 6 mW power was used, and the scattered
305 Raman signals were detected using an air-cooled multichannel charge-coupled device (CCD) detector.
306 The data acquisition time for each measurement was 30 s with 2 accumulations. The spectral
307 resolution was 1.8 cm⁻¹ using 1800 gr/mm grazing. A spatial resolution of 1 µm³ is estimated.
308 Measurements were carried out in both single point or automated imaging modes. Surfaces of 10*10
309 µm² up to 50*50 µm² with ~2 µm as a minimum step (representing 2000-5000 spectra per zone) were
310 scanned. After spectral treatment (LABSPEC6 software), the components were identified by
311 comparison with reference spectra from Raman libraries and literature data or by acquiring spectra
312 from reference materials. Complementary identification of samples was obtained from X-ray
313 diffraction (XRD) analyses. Diffractograms were obtained using a AXS D8 or D2 PHASER diffractometers
314 (Bruker) operating with Cu Kα radiation (λ = 1.54 Å). Samples were analysed at room temperature in
315 the 2θ range of 10–70°, with a step size of 0.02°.
316 Complementary, speciation of Cd, Mo, Cs and I in samples was provided by X-ray Photoelectron
317 Spectroscopy (XPS). Measurements were carried out on a Kratos Analytical AXIS Ultra^{DLD} spectrometer
318 using monochromatic Al Kα source (1486.6 eV). Calibration was performed by taking the adventitious
319 C1s peak (binding energy, BE = 285.0 eV). The uncertainties on the binding energy and on quantitative
320 elemental analysis are +/-0.1 eV and +/- 10-20%, respectively. Assignment of photoelectron peaks was
321 performed by comparison with photoelectron peaks acquired on reference compounds.

322

323 3. Results

324 3.1 Element distribution along the CHIP line and transported iodine forms

325 Element distributions are reported in Table 2 in terms of high/low temperature deposition, aerosol/gas
326 transport at 150°C (conditions of a cold leg break). Distributions are expressed in % relative to the total
327 mass injected in the high temperature (HT) zone for each element.

328 3.1.1 Nature of iodine released at 150°C

329 The sampling lines allowed to evaluate the level and nature of iodine release at 150°C for each test.
330 Results are presented in the Table 2 as gaseous form “I(gas)” and aerosol form “I(aerosol)”. The nature
331 of each form is detailed in “Iodine gas identification”, and “Iodine aerosol identification” respectively,
332 whenever it could be determined.

333 For the [In+MoCsI] test, indium was injected in excess relative to iodine (In/I~4.4), this weak excess is
334 within the range of In/I ratios observed during the Phébus FP Tests (Jacquemain *et al.*, 2000; Grégoire
335 *et al.*, 2008). Almost only gaseous iodine was released at 150 °C (“I_{aerosol&gas} line” data), with average
336 fraction close to 90% at 150°C (relative to the initial iodine mass injected in the HT zone). The molecular
337 iodine fraction can be determined from the “I₂ line” data. For this test, the sampling in the “I_{gas}
338 speciation line” failed, so that the fraction of other inorganic gaseous iodine species is determined by
339 difference between the “I_{aerosol&gas} line” and “I₂ line” data. Roughly one half of the gaseous iodine is

340 identified as molecular iodine, the rest being attributed to an inorganic form, assumed to be mostly HI
341 because the formation of HOI is less probable in such conditions (Grégoire *et al.*, 2017). Results are
342 comparable to the reference [PL_MoCsl_3] test, indicating that the presence of indium does not
343 significantly alter the chemical Mo-Cs-I-O-H system in steam atmosphere. As a consequence, it is
344 confirmed that aerosols composed of InI_x species are not formed in these experimental conditions.

345 For the [Cd+MoCsl] test, cadmium vapours were generated in a very large excess relative to iodine
346 ($Cd/I \sim 125$, much higher than observed in Phébus tests). For both " $I_{aerosol\&gas}$ line" and " I_{gas} speciation
347 line", the gaseous iodine fraction detected downstream of the aerosol filter is very low ($< \sim 1\%$). On the
348 contrary, a significant amount of gaseous molecular iodine is observed in the " I_2 line" (without inlet
349 filter), representing 28% of initially injected gaseous iodine. The fact that a measurable gaseous iodine
350 fraction could be detected only in the " I_2 line" can be accounted for by a significant retention of
351 gaseous iodine species on aerosols collected on the inlet filter of the other sampling lines. Such
352 retention was not observed during the reference [In+MoCsl] and [PL_MoCsl_3] tests, and may be due
353 to presence of cadmium species in the case of the [Cd+MoCsl] test. We thus retain the value gained
354 from the " I_2 line" (28% of initially injected iodine) for the gaseous iodine fraction. This value is
355 considered as a minimum as only I_2 fraction could be quantified in this line. The gaseous iodine fraction
356 is nevertheless almost three times lower than that observed during the [PL_MoCsl_3] reference test
357 (88.3%), indicating that cadmium species contribute to reduce the transport of gaseous iodine
358 compared to the Mo-Cs-I-O-H system in steam. Nevertheless, such cadmium effect is observed for a
359 very large Cd/I ratio.

360 The [Ag+MoCsl] test was performed with a large excess of silver relative to iodine ($Ag/I \sim 55$), thermo-
361 hydraulic conditions close to the reference test and a low level of hydrogen ($H_2/H_2O \sim 0.04$) to limit
362 possible silver oxidation. Contrarily to the tests performed with In and Cd, the " I_2 line" turned out to
363 be inefficient to trap molecular iodine (if any) in presence of metallic silver particles. Indeed, we
364 experimentally checked that silver particles react readily and quantitatively with molecular iodine
365 dissolved in toluene to form silver iodide. As a result, we retain only the data gained from the " $I_{aerosol\&gas}$
366 line" which shows a very low gaseous iodine fraction ($< 2\%$). One should keep in mind that this gaseous
367 iodine fraction may be underestimated owing to possible gaseous iodine retention on the particles
368 trapped on the inlet filter of the sampling line (similarly to the [Cd+MoCsl] test). Iodine-containing
369 particles (expected to be AgI or CsI) turned out to be mainly soluble in aqueous media suggesting that
370 formation of insoluble AgI is not the main reaction pathway leading to the release of iodine as aerosols.
371 Indeed, only 10%-25% of iodine collected in the sampling lines could be identified as AgI, that is not
372 consistent with thermochemical simulations predicting more than 75% of AgI. As a consequence, the
373 most probable iodine form to be released at 150°C is CsI.

374 Although the iodine nature at 150°C (cold leg break conditions) cannot be fully described in presence
375 of cadmium or silver, these control rod materials tend to lower the gaseous iodine fraction formed
376 along the thermal gradient.

377 **3.1.2 Element line distribution – comparison with reference test [PL MoCsl 3]**

378 Distribution of elements in the CHIP line is too coarse to allow for the identification of species
379 condensation peak. CHIP line was divided into two parts labelled as "main line": the alumina tube for
380 a temperature range of 1600-600°C and the stainless steel tube for 600-150°C (see Table 2). Except for
381 iodine, the other element found at the line outlet (at 150°C) are attributed to transport in aerosol form
382 owing to their low volatility. The following statements can be put forward based on the experimental
383 results and compared with the [PL_MoCsl_3] reference test:

384 For iodine, no deposition is observed above 600°C for all tests. Deposition below 600°C is very low
385 when iodine is mainly transported at the line outlet in gaseous form as for the [In+MoCsl] test (0.1%
386 of total injection iodine found in the 600-150°C temperature range) or the [PL_MoCsl_3] reference
387 test. When iodine is found mainly transported in aerosol form at 150°C, a significant iodine deposition
388 is observed but only below 600°C : 13% for the [Cd+MoCsl] test and 15% for the [Ag+MoCsl] test. Such

389 iodine deposition in the CHIP line results from vapour condensation or aerosol deposition of iodine
390 containing species as already observed in a previous CHIP test (Grégoire *et al.*, 2015).

391 Mo distribution in the CHIP line for the [In+MoCsl] test shows 7% deposited above 600°C, 21%
392 deposited in the 600-150°C temperature range and 72% transported as aerosols. These values are
393 comparable to that obtained for the reference test. On the contrary, in presence of Cd or Ag, Mo high
394 temperature deposition is enhanced up to 31% ([Cd+MoCsl] test) and 47% ([Ag+MoCsl] test)
395 simultaneously to a strong decrease of the deposition in the stainless steel tube (10% of Mo deposited
396 below 600°C for both tests) and to a decrease of Mo found transported at 150°C (59% for the
397 [Cd+MoCsl] test and 43% for the [Ag+MoCsl] test). This distribution is comparable to that observed for
398 the MoCsl test in steam/hydrogen (Grégoire *et al.*, 2015), in which a significant reduction of Mo(VI) to
399 the less volatile Mo(IV) and Mo(V) compounds was evidenced. Indeed reduction of Mo is not excluded
400 as oxidation of Cd or Ag in the steam flow at high temperature results in the production of low amounts
401 of hydrogen capable of reducing (even partly) the injected MoO₃ (in addition to the injected low
402 hydrogen flow for the [Ag+MoCsl] test). As consequence Mo may be less reactive to form metallic
403 molybdates and thus may contribute to the increased formation of metallic iodides (Csl, Cdl₂ and to a
404 less extent AgI).

405 Indium and silver are mainly found deposited in the high temperature zone above 600°C (alumina tube)
406 consistently with their strong refractive properties. For the [In+MoCsl] test, 42% of In is found in this
407 zone, whereas deposition below 600°C represents only 10% of initially injected In. For the [Ag+MoCsl]
408 test, 57% of silver is found deposited above 600°C and 6% below. On the contrary, cadmium which is
409 more volatile is mainly found in the 600-150°C temperature zone (41% for the [Cd+MoCsl] test and
410 less at high temperature (3% above 600°C).

411 Only caesium deposition pattern does not show significant changes in this test series: high
412 temperature deposition (above 600°C) represents 6-13% of initially injected caesium, deposition in the
413 600-150°C temperature range 13-16% so that for all test, Cs is mainly transported to the line outlet in
414 aerosol form (73-80%).

415

416
417

Table 2: [In+MoCsI], [Cd+MoCsI], [Ag+MoCsI] tests and [PL_MoCsI_3] reference test – Element distribution and iodine Gas/aerosol partition

Test Name	[In –MoCsI]	[Cd+MoCsI]	[Ag+MoCsI]	[PL_MoCsI_3] (Grégoire et al., 2015).
<u>Carrier Gas composition</u>	Ar/H ₂ O 54.3/45.7	H ₂ O/He/Ar 49.4/42.8/7.8	H ₂ O/Ar/H ₂ 49.6/48.6/1.8	H ₂ O/He/Ar 50.8/44.1/5.1
<u>Element molar Ratio in the HT zone</u>				
Cs/I	2.5 ±0.2	3.1 ±0.2	3.6 ±1.8	4.0 ±0.4
Mo/Cs	5.0 ±0.4	3.7 ±0.2	3.7 ±0.3	3.2 ±0.3
X/I (X= Cd or In or Ag)	4.5 ±0.3	126 ±9	48 ±24 ^a	
Mo/X	2.7 ±0.2	0.1 ± 0.01	0.3 ±0.02	
<u>Element molar ratio in the sampling lines</u>				
<u>At 150°C</u>				
Cs/I	2.2 ±0.5	3.1 ±0.6	~3-12	2.7 ±0.6
Mo/Cs	5.3 ±0.3	2.3 ±0.5	1.9 ±0.1	3.4 ±0.5
X/I (X= Cd or In or Ag)	2.7 ±1	48 ±23	~20-65	
<u>Deposition in the main line</u>				
	1600 -600 °C (alumina tube) and 600-150 °C (stainless steel tube)			
	0%	0%	0%	0%
I	<u>(0.1 ±0.01)%</u>	<u>(13 ±1.3)%</u>	<u>(15 ±7)%</u>	<u>(0.2 ±0.02)%</u>
Cs	(13 ±1.2)% <u>(13 ±1.2)%</u>	(10 ±0.9)% <u>(16 ±1.5)%</u>	(6 ±0.6)% <u>(14 ±0.1)%</u>	(11 ±0.9)% <u>(16 ±1.3)%</u>
Mo	(7.0 ±0.6)% <u>(21 ±2)%</u>	(31 ±2.8)% <u>(10 ±0.9)%</u>	(47 ±4.4)% <u>(10 ±0.9)%</u>	(4.0 ±0.3)% <u>(21 ±1.7)%</u>
X (X= Cd or In or Ag)	(42 ±3.8)% <u>(10 ±0.9)%</u>	(3.0 ±0.3)% <u>(41 ±3.8)%</u>	(57 ±5.4)% <u>(6.0 ±0.6)%</u>	
<u>Sampling line data: iodine transport at 150°C :</u>				
I (gas)	(89.9 ±6.5)%^b	(28 ±6.3)%^d Other lines < 1%	< (2 ±1)%^b	(88.3 ±6.4)%^{b, c}
Iodine gas identification				
I as I ₂	~ 1/2 ^d	1	nd	~ 2/3 ^{c, d}
I as HI	~ 1/2 ^{b, d}	-	nd	~ 1/3 ^{c, d}
I (aerosol)	(10 ±6.5)%^b	(59 ±6.3)%^d Other lines > 86%	> (83 ±8)%^b	(11.5 ±6.4)%^{b, c}
Iodine aerosol identification				
	nd	Traces of CdI ₂ ^e	AgI ~1/10 to 1/4 ^b	nd
<u>Sampling line data: transport of other element 150°C :</u>				
Cs (aerosol)	(74 ±2.0)%	(74 ±2.0)%	(80 ±1.5)%	(73 ±1.6)%
Mo (aerosol)	(72 ±2.0)%	(59 ±3.0)%	(43 ±4.4)%	(75 ±1.7)%
X (aerosol) (X= Cd or In or Ag)	(48 ±4.0)%	(56 ±4.0)%	(37 ±5.4)%	

418 Data rounded to two significant figures; **a**: maximum ratio as silver vaporization may also occur during the heating phase; **b** :
419 'I_{aerosol&gas} line' data; **c**: 'I_g speciation line' data; **d**: 'I₂ line' data; max. value for I_g (resp. min value for I_{aer}); **e**: Cd and I detected
420 on few particles (main line deposit -EDX examination).

421

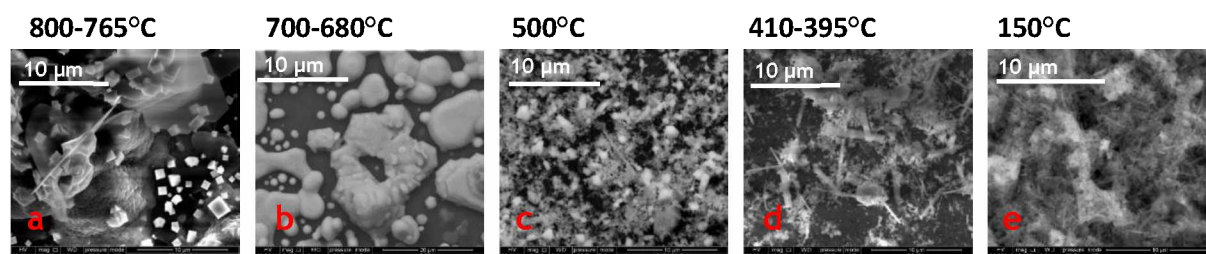
422 3.2 Characterization of condensed phase and aerosols in the 850-150 °C temperature 423 range

424 A full understanding of iodine behaviour cannot be obtained alone from sampling line data and the
425 element distribution in the line even if some first important information could be gained. In order to
426 complement these data, a detailed characterization of aerosols and/or condensed material was
427 undertaken. Both condensed deposits collected in the main line (in a temperature range from ~850°C
428 down to 350°C) and aerosols collected at 150°C were considered. Coupled analyses by SEM-EDX, RMS,
429 XPS and XRD allowed to describe morphology, element composition and to identify the main species

430 in collected condensed matter. In the following sections, analysis of deposits are detailed with
431 decreasing deposit collection temperature.

432 **3.2.1 Results for the [In+MoCs] test**

433 Deposit morphology evolution with decreasing temperature are observed by SEM in Back Scattering
434 Electron imaging (BSE) as displayed on Figure 2.



435
436 *Figure 2: [In+MoCs] test – SEM – BSE images of deposits collected in the 800-150°C temperature range*
437 *(magnification $\times 5000$ - $\times 12200$).*

438 At high temperature (800-765°C), both cubic like particles (2-3 μm) and large amorphous structures
439 can be identified (Figure 2.a). In dominates in cubic like structure whereas Si and O are found in
440 amorphous structures. Mo and Cs are found in trace amount only. RMS allows to identify the cubic like
441 particles (see Figure S2) as In_2O_3 by comparison with literature data (Kranert *et al.*, 2014). The large
442 amorphous structures observed in this temperature range are identified as melted silica with
443 characteristics Raman bands at 230 and 416 cm^{-1} (see Figure S3). Traces of mixed Cs-In polymolybdates
444 have been identified at 765°C by their Raman characteristic bands at 786 and 935 cm^{-1} (Maczka, 1997).

445 Around 700-680°C, large agglomerates of spherical or hexagonal like particles with diameter up to 10-
446 30 μm are observed together with some isolated needle-like particles (5-20 μm , not shown here)
447 (Figure 2.b). In addition to In, Cs and Mo are found as main components of the deposit with Mo/Cs
448 elemental ratio close to 3; Mo/In ratio is close to 2. For the needle like particles, the higher Mo/In
449 ratios (up to 5) indicates the possible presence of caesium molybdate species. Regarding elemental
450 ratio and RMS identification (Figure S4), $\text{CsIn}(\text{MoO}_4)_2$ is the main species identified in this temperature
451 range and appears as the large hexagonal and spherical particles 10-30 μm . Literature data predict the
452 condensation of $\text{CsIn}(\text{MoO}_4)_2$ below 650°C (Maczka, 1997) rather consistent with our experimental
453 observations. The isolated needle like particles are identified by RMS as caesium molybdates
454 ($\text{Cs}_2\text{Mo}_4\text{O}_{13}$ and $\text{Cs}_2\text{Mo}_7\text{O}_{22}$) (see Figure S5) in agreement with Hoekstra (1973) and the binary diagram
455 of CsMoO_4 - MoO_3 recently reported by Smith *et al.*, (2021).

456 Around 600°C, mixed Cs-In molybdates are still observed (not shown). In addition, indium molybdate
457 as $\text{In}_2(\text{MoO}_4)_3$ is identified (Figure S6) by comparison with spectra reported by Maczka *et al.* (2005).
458 This new species dominates deposit composition at this temperature. Given data of the MoO_3 - In_2O_3
459 binary diagram (Filipek *et al.*, 2012), indium molybdates should have been observed at higher
460 temperature (eutectic point at 780°C) indicating possible competition with the formation of the mixed
461 Cs-In molybdates (which are observed as of 765°C).

462 Below 500°C, micronic parallelepipedic particles and very fine needles (< 1 μm) are observed together
463 with larger stick like crystallites (~5-20 μm). The stick-like particle size increases as the temperature
464 decreases (Figure 2c and 2d). EDX analyses indicates a strong Mo enrichment in all particle types,
465 suggesting that Mo compounds dominates deposition. Indeed, the large sticks are mainly identified by
466 RMS as α - MoO_3 (Figure S7) (McEvoy and Stevenson, 2005; Ding *et al.*, 2006) and more sparsely
467 $\text{Cs}_2\text{Mo}_7\text{O}_{22}$. The aggregates of fine particles are tentatively attributed to molybdate species as their
468 Raman spectra feature characteristic bands in the 900-1000 cm^{-1} range typical of Mo-O vibration
469 modes. Around 500°C, $\text{In}_2(\text{MoO}_4)_3$ is found in fine crystallised needles together with two other likely
470 In/Cs molybdates but not fully attributed. At 400°C, the fine particle agglomerates are mainly
471 composed of a mixture of α - MoO_3 and $\text{Cs}_2\text{Mo}_7\text{O}_{22}$.

472 The submicronic aerosols transported at 150°C are mainly composed of CsIn(MoO₄)₂ according to the
 473 Raman and XRD data (see Figure S8) but the presence of Cs₂Mo₅O₁₆ cannot be excluded.

474 Under the oxidative atmosphere of this test (injection of steam only and indium as indium oxide),
 475 mainly Mo(VI) species were transported in the line that is confirmed by XPS (Figure S9). At 150°C, traces
 476 of reduced Mo species were observed in the aerosols (Figure S9). Similarly to the [PL_MoCsl_3] test,
 477 Mo-rich deposits are found below 600°C. Iodine was not detected in the solid samples consistently
 478 with a transport almost only under gaseous form evidenced in the previous part. A summary of the
 479 main identified species is displayed in Table 3.

480 Table 3: [In+MoCsl] test - Summary of the main identified species in the deposits and aerosols collected in the
 481 800-150°C temperature range. Dominant species are in bold characters

Analyses	800-765°C	700-680°C	600-580°C	500°C	~410-395°C	150°C
SEM-EDX						
Morphology	Cubic particles In rich In ₂ O ₃	Large hexagonal and flattened drop like particles (10- 30 μm); Cs and In rich		Micronic parallelepipedic particles Mo rich	Fine needles Mo and In-rich	Submicronic particles: mix
Elemental atomic composition and ratio	amorphous structure Si rich (fused silica) SiO ₂	Mo/In ~2 Mo/Cs ~2	Not analysed	Fine needles: In and Mo rich	Numerous large stick like crystallites Mo-rich : α-MoO ₃ and possibly (Cs/In) _x Mo _y O _z	Mo dominates Mo/In ~3 Mo/Cs ~4-5
Species		CsIn(MoO ₄) ₂		Some large stick like crystallites : α-MoO ₃ and possibly (Cs/In) _x Mo _y O _z		
RMS	In ₂ O ₃ CsIn(MoO ₄) ₂ (Cs and/or In) _x Mo _y O _z Fused silica	In ₂ O ₃ CsIn(MoO ₄) ₂ trigonal Cs ₂ MoO ₄ Cs ₂ Mo ₄ O ₁₃ (p) Cs ₂ Mo ₇ O ₂₂	In ₂ (MoO ₄) ₃ CsIn(MoO ₄) ₂ trigonal Cs ₂ Mo ₂ O ₇	In ₂ (MoO ₄) ₃ Two distinct species of the type: (Cs/In)_xMo_yO_z (Cs/In) _x Mo _y O _z Cs ₂ Mo ₂ O ₇ Cs ₂ Mo ₇ O ₂₂ (trace) α-MoO₃	In _x Mo _y O _z Cs ₂ Mo ₂ O ₇ Cs ₂ Mo ₇ O ₂₂ (trace) α-MoO₃	CsIn(MoO ₄) ₂ trigonal / CsIn(MoO ₄) ₂ orthorhombic Cs ₂ Mo ₅ O ₁₆ (consistent with XRD)

482

483 3.2.2 Results for the [Cd+MoCsl] test

484 Condensed species were analysed in the 670°C -150°C temperature range. For temperature
 485 higher than 670°C (alumina tube), very low amount of Cd-rich deposit are found (~3%, as reported in
 486 Table 3). Sizes of condensed material decrease with decreasing temperature. Large octahedrons - and
 487 rods-shaped particles are observed above 500°C when submicronic needles and ball-shaped particles
 488 are found at lower temperatures (see Figure 3a to 3e).

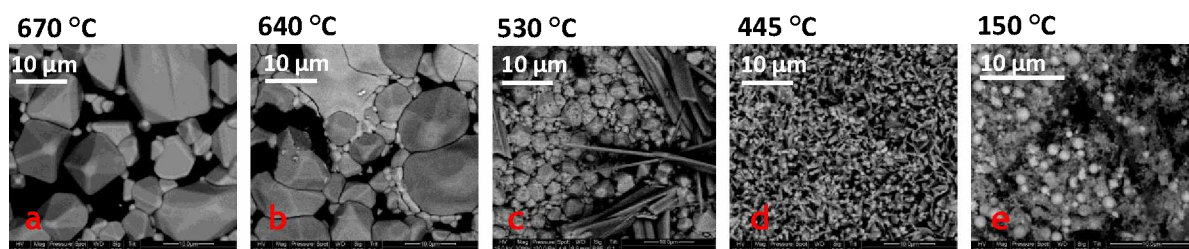


Figure 3: [Cd+MoCsI] test – SEM BSE images of deposits collected in the 670-150°C temperature range (magnification at $\times 3000$).

489
490
491

492 By comparison with Raman spectra referenced in the literature or in data bases (Ozkan *et al.*, 1990;
493 Phuruangrat *et al.*, 2011; Xing *et al.*, 2011; Tsyrenova and Pavlova, 2011), Raman spectra recorded
494 from particles is assigned to several cadmium-rich species.

495 Cadmium molybdates (mainly CdMoO_4), and mixed Cs-Cd molybdates ($\text{Cs}_2\text{Cd}_2(\text{MoO}_4)_3$) are identified
496 by RMS and XRD as main deposited species over all the 670-430°C temperature range (Figures S10,
497 S11 and S12). Additional particles composed of Cs-Cd mixed compounds as $\text{Cs}_{2x}\text{Cd}_y(\text{MoO}_4)_{x+y}$ are
498 hypothesized regarding their typical Raman line shifts but these intermediates are not described in the
499 literature. Cs-Cd molybdates may result from the reaction at high temperature between $\text{MoO}_3(\text{g})$ and
500 $\text{Cd}(\text{OH})_2(\text{g})$ and/or $\text{Cd}(\text{g})$ and $\text{CsOH}(\text{g})$. Above 600°C, the morphology of CdMoO_4 is octahedral (Shahri *et al.*,
501 2013) that is consistent with RMS results. With decreasing temperature, the overall particle size
502 decreases and the particle shape changes from octahedral to spherical. Mixed Cs-Cd molybdates are
503 observed in a cement like deposit (see Figure 3b). Cadmium silicates are identified at lower
504 temperatures (below 540°C) by EDX and XRD (Figure S12) in plate-shaped particles or rods. Reaction
505 between Cd with quartz plate substrate may account for the formation of such species.

506 The aerosols collected at 150°C are composed of aggregates of submicron particles mixed with larger
507 spherical particles (1-3 μm). CdMoO_4 and $\text{Cs}_2\text{Cd}_2(\text{MoO}_4)_3$ are the main compounds of aggregates.
508 Besides spherical particles of Cd metal, part of Cd may be also oxidized in the steam flow as $\text{Cd}(\text{OH})_2$
509 and CdO forms were detected by XRD (Figure S13). Additionally, traces of MoO_2 were also detected at
510 150°C by RMS (Figure S14). As stated in section 3.1.2, the formation of molybdenum dioxide results
511 indirectly from the oxidation of Cd metal exposed to the high temperature steam condition and
512 producing hydrogen capable of reducing MoO_3 to MoO_2 (Grégoire *et al.*, 2015). Although only
513 evidenced at the line outlet, partial reduction of Mo(VI) to Mo(IV) is consistent with high amount of
514 Mo found deposited in the high temperature zone consecutively to the formation of the less volatile
515 Mo (IV)-oxide.

516 No isolated caesium molybdate compounds are identified on any samples. The absence of such species
517 in the deposits or in the transported aerosols can result from the competition between Cs and Cd when
518 reacting with molybdenum which is in favour of the later one, since cadmium was injected in very large
519 excess with respect to Cs and Mo. Indeed, cadmium molybdate is stable in the MoO_3 -Cd system below
520 700°C with a low formation standard enthalpy (-1034 kJ/mol at 25°C - Ali *et al.*, 2005).

521 As far as iodine is concerned, no iodine containing species (such as CsI ou CdI_2) are evidenced in the
522 670°C-430°C temperature range. Low amounts of iodine are detected at 150°C by XPS (Figure S15)
523 with I 3d_{5/2} binding energy (BE) at 619.9 eV assigned to I-I bonds energy. Indeed, this BE is
524 higher than the ones expected for Cs-I or Cd-I bonds. This last feature states for I_2 likely adsorbed on
525 particles (Dillard *et al.*, 1984). Nevertheless, in presence of large amounts of Cd, the I3d_{5/2} XPS peaks
526 at 619 eV can be interfered by that of Cd3p_{3/2} (618.4 eV) so that chemical shift interpretation should
527 be considered with caution; the I 3d_{3/2} peak (631.5 eV) remains free of interference but is less
528 documented in the literature (NIST database). The characterization of the condensed material is
529 consistent with results gained from gaseous phase (organic line) strengthening the fact that interaction
530 between iodine and cadmium seems to be weaker than inferred from the Phébus FP tests (Girault and

531 Payot, 2013), even for very large excess of Cd relative to I. Table 4 summarizes the main identified
 532 species in the [Cd+MoCsI] test.

533 *Table 4: [Cd+MoCsI] test - Summary of the main identified species in the deposits and aerosols collected in*
 534 *the 800-150°C temperature range. Dominant species are in bold characters.*

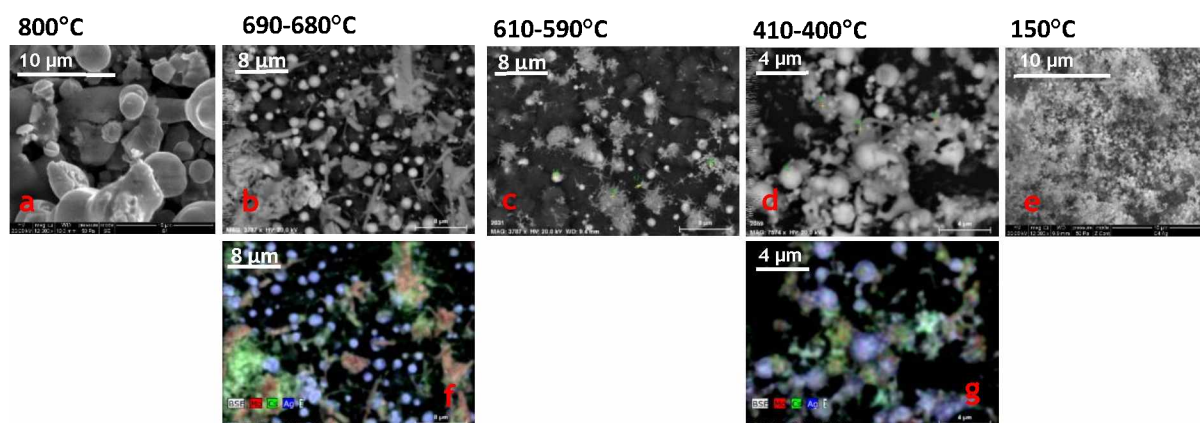
Analysis	~670°C	~640°C	~530°C	~465°C	~445°C	150°C
SEM-EDX	Octahedra Mo/Cd=1.0 CdMoO₄	Octahedra Mo/Cd=0.9 CdMoO₄	Sphere Mo/Cd=1.0 CdMoO₄	Sphere Mo/Cd=1.4 Mo/Cs=1.3 Cd/Cs=1.0 Cs₂Cd₂(MoO₄)₃	Sphere Mo/Cd=0.9 CdMoO₄	Sphere Mo/Cd=0.1 Mo/Cs=1.6 Cd/Cs=14-21
Morphology	“Cement” Mo/Cd=1.9 Mo/Cs=2.2	“Cement” Mo/Cd=1.5 Mo/Cs=1.6	Rod Cd/Si=0.9 CdSiO₃	Plate Cd/Si=1.9 Cd₂SiO₄	Plate Cd/Si=1.0 CdSiO₃	Cd Aggregate
Elemental atomic composition and ratio	Cd/Cs=1.5 Cs_{2x}Cd_y(MoO₄)_{x+y}	Cd/Cs=1.0 Cs₂Cd₂(MoO₄)₃	“Cement” Mo/Cd=1.6 Mo/Cs=1.6 Cd/Cs=1.0 Cs₂Cd₂(MoO₄)₃	Cd₂SiO₄	Sphere Mo/Cd=1.6 Mo/Cs=1.6 Cd/Cs=1.0 Cs₂Cd₂(MoO₄)₃	Mo/Cd=0.2-0.4 Mo/Cs=1.7-2.2 Cd/Cs=4.2-17 Mix
Species		Cs_{2x}Cd_y(MoO₄)_{x+y}				
RMS	CdMoO ₄ Cs ₂ Cd ₂ (MoO ₄) ₃	CdMoO ₄ Cs ₂ Cd ₂ (MoO ₄) ₃	CdMoO ₄ Cs ₂ Cd ₂ (MoO ₄) ₃ CdSiO ₃ or Cd ₂ SiO ₄	CdMoO ₄ Cs ₂ Cd ₂ (MoO ₄) ₃	CdMoO ₄ Cs ₂ Cd ₂ (MoO ₄) ₃	CdMoO ₄ Cs ₂ Cd ₂ (MoO ₄) ₃ MoO ₂
XRD	CdMoO ₄ Cs ₂ Cd ₂ (MoO ₄) ₃	CdMoO ₄ Cs ₂ Cd ₂ (MoO ₄) ₃	CdMoO ₄ Cs ₂ Cd ₂ (MoO ₄) ₃ CdSiO ₃ Cd ₂ SiO ₄	CdMoO ₄ Cs ₂ Cd ₂ (MoO ₄) ₃ CdSiO ₃ Cd ₂ SiO ₄	CdMoO ₄ Cs ₂ Cd ₂ (MoO ₄) ₃ CdSiO ₃ Cd ₂ SiO ₄	CdMoO ₄ Cs ₂ Cd ₂ (MoO ₄) ₃ Cd CdCO ₃ Cd(OH) ₂

535
 536 **3.2.3 Results for the [Ag+MoCsI] test**
 537 Various particle morphologies are identified by SEM (see Figure 4) that are observed over almost all
 538 the temperature range (800-150°C):

- 539 • Large Ag-rich spherical particles (> 10 µm) are observed both partly coalesced at high temperature
 540 and then isolated with size decreasing along with sampling temperature to reach submicronic sizes
 541 (~100 nm) at 150°C.
- 542 • Parallelepipedic crystallites (not shown) with size decreasing from ~10 µm to less than 1 µm are seen
 543 from 800°C to 150°C. EDX analyses reveal that these particles are Mo-enriched above 600 °C and
 544 featured also Ag below 600°C;
- 545 • Needle like particles are observed only when the temperature is below 700°C. The particle size
 546 varies from initially 3-4 µm long at T= 700°C to < 1µm at the temperature sampling. The needles
 547 contain mostly Mo and Ag;
- 548 • Aggregates of very fine particles are seen below 700°C, in which Cs is detected.

549 Table 5 summarizes the main identified species by combination of SEM-EDX and RMS analyses. Note
 550 that with decreasing temperature, fine particles agglomerate to form larger structures in which single
 551 components are difficult to identify. Consistently with its refractive properties, silver metal condenses
 552 early in the transport zone and is found as the main deposited species above 750°C (EDX) in the large

553 and partly coalesced droplets. Silver metal is then transported/deposited in the line as spherical
554 particles as confirmed by EDX and XRD analyses (Figure S16).



555
556 *Figure 4: [Ag+MoCsI] test - SEM-BSE (a-e) and EDX (f,g) images of deposits and aerosols collected in the*
557 *800-150°C temperature range. (on elemental images f and g: red is Mo, blue is Ag and green is Cs).*

558 In the 700-400°C temperature region, molybdenum(VI) and (IV) oxides are found by RMS as
559 predominant species. The presence of reduced forms of Mo is confirmed by XPS in the same
560 temperature range (Figure S17). The formation of MoO₂ is consistent with the injection of a low
561 amount of hydrogen and the presence of important amount of silver metal which can be considered
562 as a reducing agent. The presence of the less volatile Mo(IV) species is also consistent with enhanced
563 Mo deposition at high temperature (as stated in section 3.1). Silver molybdates (Ag₂MoO₄ as a major
564 compound and Ag₂Mo₂O₇, Ag₂Mo₃O₁₀) are also identified by RMS (Beltran *et al.*, 2014) in this
565 temperature range (Figures S18 and S19). Molybdenum oxide and silver molybdates are mostly found
566 in the needle and parallelepipedic-shaped particles. In a lesser extent caesium molybdates are also
567 identified and found as amorphous structure. Caesium molybdates account for the dominant species
568 only below 500°C. Competition between the formation of silver and caesium molybdates may explain
569 the delayed deposition of caesium molybdate species when comparing with tests featuring only the
570 Mo-Cs-I-O-H chemical system (Gouello, 2012). The distinction between silver and caesium molybdates
571 remains challenging as Raman spectra of such compounds exhibit typical Raman bands related to Mo-
572 O vibrational modes in the same spectral range (i.e. 800-100 cm⁻¹).

573 Only few single particles featuring either CsI or AgI are observed in deposits between 350°C and 400°C
574 as seen on the SEM-EDX images (Figure S20). Because iodine is injected with an elemental flow rate
575 ~50 times lower than silver one, metallic iodide (if formed) would account for a minor compound.

576
577

Table 5: [Ag+MoCsl] test - Summary of the main identified species in the deposits and aerosols collected in the 800-150°C temperature range. Dominant species are in bold characters.

Analysis	800-765°C	690-680°C	610-590°C	520-500°C	410-400°C	~350-340°C	150°C
SEM-EDX	Large spherical particles (> 5-10 µm) : Ag(0)	spherical particles (1-2 µm): Ag(0)	spherical particles (1-2 µm) : Ag(0)	Not analysed	spherical particles (1-2 µm): Ag(0)	Same as 410-400°C plate plus some Mo Rich large plates	Submicronic spherical particles (100 nm) : Ag(0)
Morphology		fine needles (~5 µm) and parallelepipedic plates (2-10 µm) : Mo rich	fine particles (<1) µm		fine particles (<1) µm		
Elemental atomic Composition		MoO ₃ , MoO ₂ and Ag ₂ MoO ₄	aggregates of fine particles around the spherical one's		aggregates of fine particles around the spherical one's		Submicronic particles difficult to characterize
Species		amorphous structure ("cement" like): Cs rich (Cs _x Mo _y O _z ?)			sparse AgI particles	sparse AgI particles	
RMS	Ag₂MoO₄ Ag ₂ Mo ₂ O ₇ Ag ₂ Mo ₃ O ₁₀	Ag₂MoO₄ Ag ₂ Mo ₂ O ₇	Ag₂MoO₄ Ag ₂ Mo ₂ O ₇ / Cs ₂ Mo ₂ O ₇ Ag ₂ Mo ₃ O ₁₀ / Cs ₂ Mo ₃ O ₁₀ (Cs/Ag) _x Mo _y O _z	Ag₂MoO₄ (Cs/Ag) _x Mo _y O _z	Ag ₂ MoO ₄	Ag ₂ MoO ₄ Ag ₂ Mo ₂ O ₇ (p)	<i>Ag₂MoO₄</i> Ag ₂ Mo ₂ O ₇ Cs/Ag _x Mo _y O _z
		Cs ₂ Mo ₂ O ₇ Cs ₂ Mo ₃ O ₁₀		Cs ₂ Mo ₂ O ₇ Cs ₂ Mo ₃ O ₁₀	Cs₂Mo₂O₇ Cs₂Mo₃O₁₀ Cs₂Mo₅O₁₆	Cs₂Mo₂O₇ Cs₂Mo₃O₁₀ Cs₂Mo₅O₁₆	Cs₂Mo₂O₇ Cs₂Mo₃O₁₀ Cs ₂ Mo ₄ O ₁₃ Cs ₂ Mo ₅ O ₁₆
	MoO ₂	MoO₃xH₂O MoO₂	MoO₂ α-MoO₃	MoO₂ MoO ₃ xH ₂ O	MoO ₃ (p) MoO ₂ (p)	MoO ₃ (p) MoO ₂ (p)	Mo _x O _y

578

579 4. Discussion

580 In the presence of SIC control rods, the behaviour of iodine may be contrasted. Iodine is transported
581 in the gaseous phase when indium is injected, but maintaining an excess of Mo with respect to Cs.
582 Whereas silver and cadmium injection in large excess induce the formation of iodide aerosols. AgI
583 formation seems to be limited despite a large excess of silver, with a formation rate lower than 10%
584 with respect to iodine ([Ag+MoCsl] test). This point confirms that AgI is less stable than CsI and CdI₂
585 consistently with thermodynamic data (Table 6). More specifically, the three tests exhibited some
586 significant differences as for iodine behaviour:

- 587 • For the [In+MoCsl] test, a part of the injected indium preferentially reacts with MoO₃ rather than
588 iodine to form indium molybdates so that InI_x formation was not observed. As Mo was injected in
589 excess of In and Cs, the molybdenum still acts as a Cs sink preventing CsI formation and thus allows
590 the existence of gaseous iodine at 150°C. It is not excluded that the injection of In₂O₃ in larger
591 amounts (e.g. larger than Mo as for the tests with Cd and Ag) could result in an increased
592 consumption of MoO₃ to form In-molybdate competing with Cs-molybdate formation and thus
593 favouring caesium iodide formation, but in any case this is not very representative of the SA case
594 (In is still in lower amount than Mo).
595
- 596 • For [Ag+MoCsl] and [Cd+MoCsl] tests, despite the injection of a huge excess of cadmium or silver
597 relative to all the other elements, the formation of metallic iodide other than CsI seems not to be
598 the main reaction pathways leading to the reduction of gaseous iodine release. Two reaction

599 pathways are put forward. Firstly, the reactivity of cadmium and silver with molybdenum oxides
 600 may contribute to significantly reduce the Cs-scavenging role of Mo by preventing the formation
 601 of caesium molybdates with Mo(VI) oxidation state. Secondly, the oxidation of the injected
 602 metallic species (Cd, Ag) may indirectly promote the formation of less reactive MoO₂ oxide. This
 603 second reaction pathway should remain limited, however, as at most 10% of injected Mo(VI) could
 604 be reduced (XPS data, see section 3.2). As a result, the formation of CsI is favoured preferentially
 605 to AgI (observed) or CdI₂ (hypothesized) in agreement with the relative stability of these
 606 compounds. Indeed, available thermodynamic data tends to show that caesium iodide is the most
 607 stable metallic iodide to be considered here both in gaseous and condensed phases.

608 *Table 6: Standard Enthalpy of formation of metallic iodide of interest taken from literature*

<i>Chemical species</i>	standard formation enthalpy for condensed species (kJ/mol)@298K	standard formation enthalpy for gaseous species (kJ/mol)@298K
<i>CsI</i>	-348.1 (Cordfunke and Prins, 1985)	-153.3 ± 1.8 (Roki <i>et al.</i> , 2014)
<i>CdI₂</i>	-205 (Konings <i>et al.</i> , 1993)	-58.8 ± 2.5 (Shugurov <i>et al.</i> , 2021)
<i>AgI</i>	-61.8 (Taylor and Anderson, 1921)	125.3 (Barin, 1989)
<i>InI</i>	-102 (Vasil'ev <i>et al.</i> , 1987)	26.4 (Gurvich <i>et al.</i> 1989)
<i>InI₃</i>	-223 (Vasil'ev <i>et al.</i> , 1987)	-105.4 (Gurvich <i>et al.</i> 1989)

609
 610 Characterization of the main compounds deposited in the CHIP line allowed for identifying several
 611 metallic polymolybdates in addition to the caesium molybdates already characterized in similar
 612 thermal hydraulic conditions (Lacoue-Nègre, 2010; Gouello *et al.*, 2013; Grégoire *et al.*, 2015). Such
 613 species were not mentioned for the VERCORS nor Phébus tests. Nevertheless, deposition profile of In,
 614 Cs and Mo obtained in a 800-200°C thermal gradient for the VERCORS HT tests (deposition along
 615 Thermal Gradient Tube as reported by Pontillon and Ducros, 2010) showed concomitant deposition in
 616 the ~800°C (HT2 test), ~675-725°C (HT3 test) and ~640°C (HT2 test) temperature zones, so that
 617 deposition of metallic molybdates involving Cs and/or In cannot be excluded. Silver deposition is much
 618 more complex to discuss featuring a low homogeneous deposition detected below 700°C (HT3 test)
 619 and 600°C (HT2 test) and no data for Cd deposition is available. As only I and Cs deposition profiles
 620 were determined for the Phébus Thermal Gradient Tube (700-200 °C) during the FPT1 and FPT2 tests
 621 (Girault and Payot, 2013), it will be difficult to infer any comparison with our results.

622 The formation of various metallic polymolybdates entering in competition with the formation of
 623 caesium polymolybdates is clearly evidenced in the three tests. Indeed, deposits containing pure
 624 caesium molybdates were detected at a lower temperatures (below 600°C for [In+MoCsI] and
 625 [Ag+MoCsI] tests) than observed when only Mo oxide and Cs species are reacting together (1000°C, as
 626 reported in Gouello *et al.*, 2013). Cd and Ag are injected both in large excess relative to Mo and Cs, so
 627 that a direct comparison of the two tests in terms of molybdate formation can be put forward. Pure
 628 caesium molybdates are still observed in [Ag+MoCsI] test, as well as MoO₂ and MoO₃ species. On the
 629 contrary, cadmium-containing molybdates are the dominant species in the [Cd+MoCsI] test featuring
 630 only mixed CdCs molybdates and traces of MoO₂ (aerosols collected at the line outlet). These features
 631 indicate that the formation silver molybdates seem less favoured compared to that of cadmium
 632 molybdates in our test condition. Even if In₂O₃ was injected in lower amount (in default relative to Mo
 633 but in excess compared to Cs), the formation of indium molybdates seem favoured at high
 634 temperature, compared to that of pure caesium molybdates, as CsIn(MoO₄)₃ and In₂(MoO₄)₃ are the
 635 dominant species in the 500-750°C temperature range. Caesium was found mainly as a mixed InCs
 636 molybdate compounds over all the temperature range, pure caesium molybdates appearing less
 637 abundant. In the oxidative atmosphere of this test (steam injection and no reducing species), the

638 excess Mo was found mainly as α -MoO₃ from 500°C down. It is nevertheless difficult to know exactly
 639 if the species are formed in the gas phase and/or in the solid phase after condensation of In, Mo and
 640 Cs species in oxide or hydroxide forms.

641 Formation enthalpies referenced in the literature show that caesium molybdates are most stable
 642 compared to cadmium, silver and indium molybdates even if the thermodynamic data are uncomplete
 643 with no mixed elements (see Table 7). In our conditions the large excess of Cd, Ag and In reagents
 644 compared to Cs may have displaced equilibrium in favour of Cd, Ag or In-molybdates in the high
 645 temperature zone. Consumption of these elements results in the formation of the more stable Cs
 646 molybdates at lower temperature as experimentally observed. In this discussion, possible kinetic
 647 limitations in the thermal-hydraulic transient are not taken into account and thermodynamic data are
 648 nevertheless not all available in the literature.

649 *Table 7: Standard Enthalpy of formation of molybdates of interest taken from literature*

Chemical species	standard formation enthalpy for condensed species (kJ/mol)@298K	standard formation enthalpy for gaseous species (kJ/mol)@298K
α -MoO ₃ (s) and MoO ₃ (g)	-745.5 (Crouch-Baker and Dickens, 1984)	-364.4 ± 20.0, (Cordfunke and Konings, 1990)
Cs ₂ MoO ₄	-1514.4 (Gamsjäger and Morishida, 2015)	-1179.2 (Tangri <i>et al.</i> , 1989)
In ₂ MoO ₄	Not available	-855 ± 33 (Lopatin <i>et al.</i> , 2013)
Ag ₂ MoO ₄	-838.2 (Gamsjäger and Wiessner, 2018; Gamsjäger and Morishita, 2015)	-459.6 (CCSD(T)/CBS(TZ-QZ) value, method described in Saab and Souvi, 2018)
CdMoO ₄	-1034 ± 5.7 ; -1015.4 ± 14.5 Ali <i>et al.</i> , 2005 ; Mishra <i>et al.</i> , 2006	-606.0 (CCSD(T)/CBS(TZ-QZ) value, method described in Saab and Souvi, 2018)
SnMoO ₄	Not available	-699 ± 29 (Shugurov <i>et al.</i> , 2015)

650
 651 Even if trends could be inferred from a direct comparison of stability of the identified compounds, a
 652 full understanding of the main reactions which occurred in the CHIP line with these chemical systems
 653 will be gained by simulation of the experiments with severe accident calculation codes as
 654 ASTEC/SOPHAEROS (Cousin *et al.*, 2008; Cantrel *et al.*, 2013). Nevertheless, up to date, thermodynamic
 655 data of some metallic molybdates evidenced in these experiments are not available in the literature
 656 and cannot be accounted in the thermodynamic database of the simulation tools. Density Functional
 657 Theory calculations may help to provide some of the missing thermodynamic data for gaseous species.

658

659 5. Conclusion

660 A series of tests performed in the CHIP line with the Mo-Cs-I-O-H chemical system and CR elements
 661 revealed that the behaviour of each component (Ag, In and Cd) of the SIC control rod considered
 662 separately is much more complex than initially expected. Indeed, combined on-line sampling,
 663 elemental post-test analyses and an extended characterization of deposits allow for identifying most
 664 of formed compounds during the transport in the thermal gradient (1600-150°C) of the CHIP line.
 665 These species could not be evidenced in the larger scale Phébus tests or VERCORS HT tests.

666 In the case of indium injection, a release of gaseous iodine similar to the [PL_MoCsI_3] reference test
 667 is observed. Indium iodide formation is not observed as expected from the low stability of InI_x(g). The
 668 fully oxidative conditions contribute to maintain Mo in the +VI oxidation state and thus its capabilities
 669 to easily form metallic molybdates. Beside, significant deposition of In₂O₃ at high temperature (>750°C)
 670 owing to the refractive behaviour of this species, the main contribution of In injection is the formation

671 of indium and mixed In-Cs molybdates likely in the condensed phase. Owing to the large excess of Mo
672 relative to both In and Cs, Mo still plays a Cs-sink role with a large fraction of gaseous iodine
673 transported at low temperature.

674 In the case of both cadmium and silver injection, the formation of metallic iodide other than CsI seems
675 not to be the main reaction pathways leading to a strong reduction of gaseous iodine release despite
676 the injection of a very large excess relative to all the other elements (I, Cs and Mo). The formation of
677 various metallic silver or cadmium molybdates entering in competition with caesium molybdates
678 contribute to significantly reduce the Cs-scavenging role of Mo.

679 It can be stated that due to the high stability of caesium iodide, only the absence of Cs can prevent its
680 formation but if caesium molybdates are formed, as detailed before, caesium cannot be totally
681 consumed by molybdenum in presence of control rod materials.

682 It is worth noting that all these results apply to the CHIP conditions where molybdenum is injected in
683 slight excess and silver and cadmium in large excess with respect to representative conditions of a
684 severe accident.

685 Efforts are ongoing to improve the ASTEC/SOPHAEROS modelling to reproduce as much as possible all
686 the trends experimentally observed in terms of iodine chemical reactivity and also FPs deposits, to be
687 at least capable to deepen the understanding of the FP's chemistry observed during the Phébus tests
688 (Girault and Payot, 2013) and later on perform SA simulations

689

690 CRediT authorship contribution statement

691 Grégoire A.C.: Investigation, Writing - original draft; Sobanska S : Investigation, Writing - original draft,
692 Tornabene C.: Investigation; Talaga D.: Investigation; Mamede A.S.: Investigation; Morin S.:
693 Investigation; Cantrel L. : Writing, original draft.

694 Declaration of Competing Interest:

695 The authors declare that they have no known competing financial interests or personal relationships
696 that could have appeared to influence the work reported in this paper.

697

698 Acknowledgements

699 This work was performed in the frame of the experimental CHIP+ programme with the financial
700 support of EDF. The authors thank the Labex Cappa (ANR-11-LABX-0005-01) for funding XPS analyses
701 performed at the 'plateforme d'analyses de surfaces' of the Lille University. The *Fonds Européen de*
702 *Développement Régional* (FEDER), *CNRS*, *Région Nord Pas-de-Calais* and *Ministère de l'Éducation*
703 *Nationale de l'Enseignement Supérieur et de la Recherche* are acknowledged for fundings of
704 XPS/LEIS/ToF-SIMS spectrometers. Analyses performed at the Institute of Molecular Science of
705 Bordeaux University were supported the IRSN/ADERA contract n°12033756. E. Assaf and G. Montaud
706 are acknowledged for their participation in the RMS measurements of condensed phase samples. We
707 thank P. Recourt from LOG UMR CNRS 8187 (Lille University) for SEM-EDX measurements of
708 [Cd+MoCsI] test samples. LASIR UMR 8516 (Lille University) is acknowledged for making the RMS
709 equipment available for measuring [Cd+MoCsI] test samples.

710

- 711 Glossary:
- 712 ASTEC: Accident Source Term Evaluation Code
- 713 BSE : Back Scattering Electron imaging
- 714 CHIP : Chemistry Iodine Primary circuit
- 715 EdF : Electricité de France
- 716 ESEM-EDX: Environmental Scanning Electron Microscopy – Energy Dispersive X-ray Spectroscopy
- 717 FD NPP: Fukushima Daiichi Nuclear Power Plants
- 718 FP: Fission Product
- 719 FPs : Fission Products
- 720 GAEC : Generation of AErosols in the reactor Coolant system
- 721 ICP AES: Inductively Coupled Plasma – Atomic Emission Spectroscopy
- 722 ICP MS: Inductively Coupled Plasma – Mass Spectrometry
- 723 LWR : Light Water Reactor
- 724 PWR: pressurised Water reactor
- 725 RCS: reactor Coolant System
- 726 RMS : Raman Micro Spectrometry
- 727 SA: Severe Accident
- 728 SE : Secondary Electron imaging
- 729 SIC CR : Silver-Indium-Cadmium Control Rod
- 730 XRD: X-Ray Diffraction
- 731

732 References

- 733 Ali (Basu) M, Bharadwaj S R, Das D. (2005). The standard molar enthalpy of formation of CdMoO₄, Journal
734 of Nuclear Material, 336, 110-112. doi:10.1016/j.jnucmat.2004.09.006
- 735 Barin I. (1989), Thermochemical Data of Pure Substances, VCH, Weinheim.
- 736 Beahm E. C., Weber C.F., Kress T. S., Parker, G. W. (1992). Iodine Chemical Forms in LWR Severe Accidents –
737 Final Report, NUREG/CR-5732 – ORNL/TM-11861.
- 738 Beltran A., Gracia L., Longo E., Andres J. (2014). First-principles study of pressure-induced phase transitions
739 and electronic properties of Ag₂MoO₄, Journal of Physical Chemistry C, 118, 3724-3732.
740 doi:10.1021/jp4118024
- 741 Bowsler B.R. and Dickinson, S. (1986). The interaction of caesium iodide with boric acid: vapour phase and
742 vapour condensed phase reactions, 1986, AEE-Winfrith R-2102.
- 743 Bowsler, B.R. and Nichols, A.L. (1985) High temperature studies of simulant fission products: Part IV,
744 Interaction of caesium iodide with boric acid over the temperature range 400 to 1000 °C, AEE-Winfrith R-
745 1973.
- 746 Cantrel L., Louis F., Cousin F. (2013). Advances in mechanistic understanding of iodine behaviour in Phebus-
747 FP tests with the help of ab-initio calculations, Annals of Nuclear Energy, 61, 170-178. doi:
748 10.1016/j.anucene.2013.02.034
- 749 Chino M., Nakayama H., Nagai H., Terada H., Gatata G., Yamazawa H. (2011) Preliminary estimation of release
750 amounts of I-131 and Cs-137 accidentally discharged from the Fukushima Daiichi nuclear power plant into
751 the atmosphere, Journal of Nuclear Science and Technology, 48, 1129-1134. doi:
752 10.1080/18811248.2011.9711799
- 753 Clément B. and Zeyen R. (2005). The Phébus Fission Product and Source Term International Programs. Proc.
754 Int. Conf. on Nuclear Energy for New Europe, Bled, Slovenia, 5-8 September, Nuclear Society of Slovenia.
- 755 Clément B. Cantrel L., Ducros G., Funke F., Herranz L., Rydl A., Weber G., Wren C. (2007). State of the art
756 report on iodine chemistry, NEA/CSNI/R(2007)1.
- 757 Cordfunke E.H.P. and Prins G. (1985). The thermochemical properties of caesium iodide. I thermodynamic
758 functions of solid CsI, Thermochemica Acta, 90, 169-176. doi: 10.1016/0040-6031(85)87094-5
- 759 Cordfunke, E. H. P.; Konings, R. J. M. (1990). Thermochemical Data for Reactor Materials and Fission Products;
760 Elsevier: Amsterdam.
- 761 Cousin F., Dieschbourg K., Jacq F. (2008). New capabilities of simulating fission product transport in circuits
762 with Astec/Sophaeros V.1.3., Nuclear Engineering and Design, 238 (9), 2430–2438. doi:
763 10.1016/j.nucengdes.2008.03.018
- 764 Crouch Baker S. and Dickens P.G. (1984). Standard molar enthalpy of formation of a-MoO₃-H₂O by solution
765 calorimetry, Journal of Chemical Thermodynamics, 16, 301-302. doi: 10.1016/0021-9614(84)90093-4
- 766 De Boer, R. and Cordfunke, E.H.P. (1995). On the Caesium rich part of the Cs-Te phase diagram, Journal of
767 Alloys and Compounds, 228, pp 75-78. doi: 10.1016/0925-8388(95)01666-X
- 768 Dillard G., Moers. H., Klewe-Nebenius H., Kirch G., Pfennig G. And Ache H.J. (1984). The absorption of methyl
769 iodide on uranium and uranium dioxide: surface characterisation using X-ray photoelectron spectroscopy,
770 Surface Science, 145, 62-86. doi: 10.1016/0039-6028(84)90766-0
- 771 Ding, Q. P., Huang, H. B., *et al.* (2006). "Molybdenum trioxide nanostructures prepared by thermal oxidation
772 of molybdenum." Journal of Crystal Growth 294(2): 304-308. doi : 10.1016/j.jcrysgro.2006.07.004 .
- 773 Elrick R.M., *et al.* (1987). Boron Carbide – Steam Reactions with Cesium hydroxide and with Cesium Iodide
774 at 1270 K in an Inconel 600 system, NUREG CR-4963, SAN87-1491.
- 775 Filipek E., Rychlowska-Himmel I. Paczesna A. (2012). Thermal stability of In₂(MoO₄)₃ and phase equilibria in
776 the MoO₃-In₂O₃ system, Journal of Thermal Analysis and Calorimetry, 109, 711-716. doi: 10.1007/s10973-
777 012-2224-7.

778 Gamsjäger E. and Wiessner M. (2018). Low temperature heat capacities and thermodynamic functions
779 described by Debye–Einstein integrals, *Monatshefte für Chemie*, 149, 357–368. doi: 10.1007/s00706-017-
780 2117-3.

781 Gamsjäger H. and Morishita, M. (2015). Thermodynamic properties of molybdate ion: reaction cycles and
782 experiments, *Pure Applied Chemistry*, 87(5), 461-476. doi: 10.1515/pac-2014-1105.

783 Geng X., Xie Z., Zhang L. (2017) Influence of emission rate on atmospheric dispersion modeling of the
784 Fukushima Daiichi Nuclear Power Plant accident, *Atmospheric Pollution Research*, 8, 439-445. doi:
785 10.1016/j.jenvrad.2016.01.011

786 Girault N. and Payot F. (2013). Insights into iodine behaviour and speciation in the Phébus primary circuit,
787 *Annals of Nuclear Energy*, 61, pp 143–156, doi: 10.1016/j.anucene.2013.03.038

788 Girault N., Bosland L., Dickinson S., Funke F., Güntay S., Herranz L.E., Powers D., (2012). LWR severe accident
789 simulation: Iodine behaviour in FPT2 experiment and advances on containment iodine chemistry, *Nuclear
790 Engineering and Design*, 243, 371-392, doi: 10.1016/j.nucengdes.2011.11.011

791 Girault N., Bosland L., Dienstbier J., Dubourg R., Fiche C. (2010). LWR severe accident simulation fission
792 product behavior in FPT2 experiment, *Nuclear Technology*, 169, 218-238. doi: 10.13182/NT10-A9375

793 Gouello M. (2012). Chemistry of iodine and aerosol composition in the primary circuit of a nuclear plant in
794 severe accident conditions, Ph-D, University J. Fourier, Grenoble (in French).

795 Gouello M., Mutelle H., Cousin F., Sobanska S., Blanquet E. (2013). Analysis of the iodine gas phase produced
796 by interaction of CsI and MoO₃ vapours in flowing steam, *Nuclear Engineering and Design* 263, 462– 472. doi:
797 10.1016/j.anucene.2013.06.016

798 Grégoire A.C. and Haste T. (2013). Material release from the bundle in Phébus FP, *Annals of Nuclear Energy*,
799 61, 63–74. doi: 10.1016/j.anucene.2012.02.037

800 Grégoire A.C., Délicat Y., Tornabene C., Cousin F., Gasnot L. Lamoureux N., Cantrel L. (2017). Study of the
801 iodine kinetics in thermal conditions of a RCS in nuclear severe accident, *Annals of Nuclear Energy* 101, 69-
802 82. doi: 10.1016/j.anucene.2016.10.013

803 Grégoire A.-C., Kalinainen J., Cousin F., Mutelle H., Cantrel L., Auvinen A., Haste T., Sobanska S. (2015).
804 Studies on the role of molybdenum on iodine transport in the RCS in nuclear severe accident conditions,
805 *Annals of Nuclear Energy*, 78, 117–129. doi: 10.1016/j.anucene.2014.11.026

806 Grégoire A.C., March P., Payot F., Zabiego M., De Bremaecker A, Biard B., Schlutig S., Grégoire G. (2008).
807 FPT2 Final report, (IPSN) - PH-PF report IP/08/579.

808 Grégoire A.C., Morin S., Cantrel L. (2018). Main outcomes of the IRSN experimental CHIP and CHIP+
809 programmes in Proc. of Conference Nuclear Energy for New Europe, 2018, Portoros 10-13 September
810 (Slovenia). Communication.

811 Grégoire A.C., Mutelle H. (2012). Experimental Study of the [B, CS, I, O, H] and [Mo, Cs, I, O, H] Systems in
812 the Primary Circuit of a PWR in Conditions Representative of a Severe Accident in Proc. Of Conference
813 Nuclear Energy for New Europe, Ljubljana 5-7 September (Slovenia).

814 Gurvich L.V., Veyts I.V., Alcock C.B. (1989). *Thermodynamic Properties of Individual Substances - 4th edition.*

815 Haste T., Payot F., Bottomley P.D.W. (2013). Transport and deposition in the Phébus FP circuit, *Annals of
816 Nuclear Energy*, 61, 102-121. doi: 10.1016/j.anucene.2012.10.032

817 Haste T., Payot F., Bottomley P.D.W. (2013). Transport and deposition in the Phébus FP circuit, *Annals of
818 Nuclear Energy*, 61, 102-121. doi: 10.1016/j.anucene.2012.10.032

819 Hoekstra H.R. (1973). The Cs₂MoO₄-MoO₃ system, *Inorganic and Nuclear Chemistry Letters*, 9, pp 1291-1301.
820 doi: 10.1016/0020-1650(73)80013-3

821 Hoeve J.E.T., Jacobson M.Z. (2012). Worldwide health effects of the Fukushima Daiichi nuclear accident,
822 *Energy and Environmental Science*, 5, 8743-8757. doi: 10.1039/C2EE22019A

823 Huh C., Hsu S., Lin C. (2012) Fukushima-derived fission nuclides monitored around Taiwan: free tropospheric
824 versus boundary layer transport, *Earth and Planetary Science Letters*, 319, 9-14. doi:
825 10.1016/j.epsl.2011.12.004

826 Jacquemain D., Bourdon S., De Bremaecker A., Barrachin M., (2000). FPT1 Final report, (IPSN) - PH-PF report
827 IP/00/479.

828 Jacquemain D., coordinator (2015). Nuclear Power Reactor Core Melt Accident, Current state of
829 knowledge, edp science, ISBN: 978-2-7598-1835-8. [https://www.edp-](https://www.edp-open.org/images/stories/books/fullIdl/Nuclear_Power_Reactor_Core_Melt_Accidents.pdf)
830 [open.org/images/stories/books/fullIdl/Nuclear_Power_Reactor_Core_Melt_Accidents.pdf](https://www.edp-open.org/images/stories/books/fullIdl/Nuclear_Power_Reactor_Core_Melt_Accidents.pdf).

831 Konings R.J.M, Cordfunke E.H.P., Ouweltjes W. (1993). The standard molar enthalpies of formation of CdI₂(s)
832 and Cs₂Cd₂I₄(s). *Journal of Chemical Thermodynamics*, 25, 271-276. doi :10.1006/jcht.1993.1026

833 Kranert C., Schmidt Grund R., Gundman M. (2014). Raman Active Phonon modes of cubic In₂O₃, *Phys Status*
834 *Solidii RRI*, 6, 554-559. doi: 10.1002/pssr.201409004

835 Lacoue Nègre M. (2010). Iodine chemistry in the reactor coolant system of a nuclear power plant in case of
836 a severe accident – study of CsI/MoO₃ mixture under steam, Ph-D, university USTL, Lille (in French).

837 Lebel L.S., Dickson R.S., Glowa G.A. (2016). Radioiodine in the atmosphere after the Fukushima Dai-ichi
838 nuclear accident. *Journal of Environmental Radioactivity*, 151, pp 82-93. doi: 10.1016/j.jenvrad.2015.06.001.

839 Lopatin S.I., Panin A.I. , Shugurov S.M (2013). Stability and structures of gaseous In₂MoO₄, In₂WO₄ and
840 In₂W₂O₇, *Dalton Transactions*, 42, 8339–8346 . doi: 10.1039/c3dt32719a

841 Maczka M. (1997). Vibrational Characteristics of the alkali metal-indium double molybdate M-In(MoO₄)₂ and
842 tungstate M-In(WO₄)₂ (M=Li, Na, K, Cs), *Journal of Solid State Chemistry*, 129, 287-297. doi:
843 10.1006/jssc.1996.7248

844 Maczka M., Hermanowicz K., Hanuza J. (2005). Phase transition and vibrational properties of A₂(BO₄)₃
845 compounds (A=Sc, In; B=Mo, W), *Journal of Molecular Structure*, 744-747, 283-288. doi :
846 1016/j.molstruct.2004.10.049

847 Masson O., Tschiersch J., Lebel L.S., Wershofen H., Mietelski J.W., Steinhäuser G., Blanchardon E., Cantrel L.,
848 Grégoire A.C., Quélo D. (2019), Radio-iodine release in : Nuclear Emergencies (Book) , Chap 15, Ed G.
849 Steinhäuser, A Koizumi, K Shozugawa, ISSN 2364-8333 ISSN 2364-8341. doi: 10.1007/978-981-13-8327-4

850 Masson, O. *et al.* (2011). Tracking of airborne radionuclides from the damaged Fukushima Dai-Ichi nuclear
851 reactors by European Networks. *Environ. Sci. Technol.*, 45, pp 7670–7677. doi :10.1021/es2017158

852 McEvoy T. M. and Stevenson K. J. (2005). "Spatially Resolved Imaging of Inhomogeneous Charge Transfer
853 Behavior in Polymorphous Molybdenum Oxide. I. Correlation of Localized Structural, Electronic, and
854 Chemical Properties Using Conductive Probe Atomic Force Microscopy and Raman Microprobe
855 Spectroscopy." *Langmuir* 21(8): 3521-3528. doi : 10.1021/la047276v

856 McFarlane J. and Leblanc, J.L. (1996). Fission product Tellurium and Cesium telluride. Chemistry revisited.
857 AECL report 11333 COG 95-L76-I.

858 McFarlane J., Wren J.-C., Lemire R.J. (2002). Chemical speciation of iodine source term to containment,
859 *Nuclear Technology*, 138, 162-178. doi: 10.13182/NT138-162

860 Mishra R., Bharadwaj S. R., Das D. (2006). DETERMINATION OF THERMODYNAMIC STABILITY OF CdMoO₄ BY
861 KNUDSEN EFFUSION VAPOR PRESSURE MEASUREMENT METHOD, *J Therm Anal Calorim.* 86, 547–552. doi:
862 10.1007/s10973-005-7285-4

863 Miyahara N., Miwa,S., Horiguchi N., Sato I., Masahiko O. (2019). Chemical reaction kinetics dataset of Cs-I-
864 B-Mo-O-H system for evaluation of fission product chemistry under LWR severe accident conditions. *J. of*
865 *Nuclear Science and Technology* 56(2), 228-240.

866 Ozkan U.S., Gill R.C., Smith M.R. (1990). Synergy in CdMoO₄/MoO₃ catalysts in partial oxidation reactions of
867 C₄ hydrocarbons, *Applied Catalysis*, 62, 105-117. doi: 10.1016/S0166-9834(00)82240-X

868 Phuruangrat A., Ekthammathat, E., Thongtem T., Thongtem S. (2011). Microwave-assisted synthesis and
869 optical property of CdMoO₄ nanoparticles, *Journal of Physics and Chemistry of Solids* 72, Issue 3, 176–180.
870 doi: 10.1016/j.pcs.2010.12.003

871 Pontillon Y. and Ducros G (2010). Behaviour of fission products under severe PWR accident conditions The
872 VERCORS experimental programme—Part 2: Release and transport of fission gases and volatile fission
873 products, *Nuclear Engineering and Design*, 240 (2010) 1853–1866. doi:10.1016/j.nucengdes.2009.06.024

874 Roki F.-Z., Ohnet M.-N., Fillet S., Chatillon C., Nuta I. (2014). Critical assessment of thermodynamic properties
875 of CsI solid, liquid and gas phases. *Journal of Chemical Thermodynamics* 70, 46-72. doi:
876 10.1016/j.jct.2013.09.038

877 Saab M., Souvi S (2018). Quantum Modelling of AgHMoO₄, CsHMoO₄ and AgCsMoO₄ Chemistry in the Field
878 of Nuclear Power Plant Safety, *International Journal of Chemical and Molecular Engineering* 12(5), 244-248.
879 doi: 10.5281/zenodo.1317244

880 Shahri Z., Sobhani A., Salavati-Niasari, M. (2013). Controllable synthesis and characterization of cadmium
881 molybdate octahedral nanocrystals by coprecipitation method, *Materials Research Bulletin* 48, 3901–3909.
882 doi: 10.1016/j.materresbull.2013.05.100

883 Smith A.L., Vlieland J., Pignié M.C., Abbink M., Mikaelian G., Benigni P. (2021). New insights into the Cs-Mo-
884 O system: Experimental studies of the Cs₂MoO₄-MoO₃ pseudo-binary system, *Thermochimica Acta* 696,
885 178825. doi: 10.1016/j.tca.2020.178825

886 Spies J.R.(1936). Process for obtaining free silver and iodine from silver iodide, Patented n°2,060,539.

887 Shugurov S.M., Panin A.I., Lopatin S.I., Emelyanova K.A. (2015). Thermodynamic study of gaseous tin
888 molybdates by high-temperature mass spectrometry, *Rapid Communications in Mass Spectrometry* 29(5),
889 1427-1436. doi: 10.1002/rcm.7237

890 Shugurov S.M., Panin A.I., Lopatin S.I., Panaeva M.A. (2021). Vapor pressures and thermodynamic properties
891 of simple and complex iodides. *Thermochimica Acta* 703, 178996. doi: 10.1016/j.tca.2021.178996

892 Stohl A., Seibert P., Wotawa G., Arnold D., Burkhart J. F., Eckhardt S., Tapia C., Vargas A., Yasunari T.J. (2012
893) Xenon-133 and caesium-137 releases into the atmosphere from the Fukushima Dai-ichi nuclear power
894 plant: determination of the source term, atmospheric dispersion, and deposition, *Atmospheric Chemistry
895 and Physics*, 12, 2313-2343. doi: 10.5194/acp-12-2313-2012.

896 Tangri R.P., Venugopal V., Bose D.K., Sundaresan M. (1989). Thermodynamics of vaporisation of caesium
897 molybdate, *Journal of Nuclear Materials* 167, 127-130. doi: 10.1016/0022-3115(89)90433-9

898 Taylor H.S. and Anderson W.T. (1921). The heat of formation of silver iodide, *Journal of the American
899 Chemical Society* , 43 (9), 2014–2017. doi: 10.1021/ja01442a004

900 Tsyrenova G. D. and Pavlova N. N. (2011). Synthesis, Structure, and Electrical and Acoustic Properties of
901 Cs₂Cd₂(MoO₄)₃, *Inorganic Materials*, 47(7), 786–790. doi: 10.1134/S0020168511070235

902 Vasil'ev, Ya.V.; Matskevich, N.I.; Stenin, Yu.G. (1987). New determination of enthalpies of indium tri- and
903 monoiodide formation. Massive adiabatic calorimeter, *Izvestiya Sibirskogo Otdeleniya Akademii Nauk SSSR,
904 Seriya Khimicheskikh Nauk*; ISSN 0002-3426; CODEN IZSKA; (no.2); p. 3-8

905 Wang Y.L., Nagy J.C., Margerum D.W. (1989). Kinetics of hydrolysis of iodine monochloride measured by the
906 pulsed-accelerated-flow method, *Journal of the American Chemical Society*, 111, 7838-7844.
907 doi :10.1021/ja00202a026

908 William D.A. (1994). OECD International Standard Problem Number34 Falcon Code Comparison Report,
909 NEA/CNSI/R(94)27.

910 Xing G. Xu y., Zhao C., Wang Y. Li Y., Wu Z., Liu T. Wu G. (2011). Photoluminescence properties of CdMoO₄
911 disk and hollow microsphere-like crystals synthesized by hydrothermal conventional method. *Powder
912 Technology*, 213, 109–115. doi: 10.1016/j.powtec.2011.07.012